



저작자표시-비영리-변경금지 2.0 대한민국

이용자는 아래의 조건을 따르는 경우에 한하여 자유롭게

- 이 저작물을 복제, 배포, 전송, 전시, 공연 및 방송할 수 있습니다.

다음과 같은 조건을 따라야 합니다:



저작자표시. 귀하는 원저작자를 표시하여야 합니다.



비영리. 귀하는 이 저작물을 영리 목적으로 이용할 수 없습니다.



변경금지. 귀하는 이 저작물을 개작, 변형 또는 가공할 수 없습니다.

- 귀하는, 이 저작물의 재이용이나 배포의 경우, 이 저작물에 적용된 이용허락조건을 명확하게 나타내어야 합니다.
- 저작권자로부터 별도의 허가를 받으면 이러한 조건들은 적용되지 않습니다.

저작권법에 따른 이용자의 권리는 위의 내용에 의하여 영향을 받지 않습니다.

이것은 [이용허락규약\(Legal Code\)](#)을 이해하기 쉽게 요약한 것입니다.

[Disclaimer](#)

Master's Dissertation

# Design and Synthesis of Carbon-based Porous Organic Networks

Sun-Hee Shin

Department of Energy Engineering

Graduate School of UNIST

2018

# Design and Synthesis of Carbon-based Porous Organic Networks

Sun-Hee Shin

Department of Energy Engineering

Graduate School of UNIST

# Design and Synthesis of Carbon-based Porous Organic Networks

A dissertation  
submitted to the Graduate School of UNIST  
in partial fulfillment of the  
requirements for the degree of  
Master of Science

Sun-Hee Shin

06. 14. 2018

Approved by



---

Advisor

Jong-Beom Baek

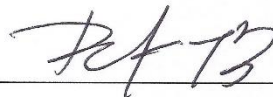
# Design and Synthesis of Carbon-based Porous Organic Networks

Sun-Hee Shin

This certifies that the dissertation of Sun-Hee Shin is approved.

06 / 14 / 2018

Signature



Advisor: Jong-Beom Baek

Signature



typed name: Hu Young Jeong #1

Signature



typed name: In-Yup Jeon #2

## Abstract

The synthesis of carbon-based heteroatom doped materials attracted many interests as well as its unique, extraordinary and controllable chemical/physical properties which can drive their infinite potential applications. Extended synthetic approaches for new materials allows that improve processability and performance to utilize its own superiority to the maximum. In here, research overview and objective carried out during my master's degree, will be discussed.

The dissertation consists of mainly two chapters: 1) Design and synthesis of two-dimensional sheet-like BBL structure (2D-BBLs). The 2D-BBLs were successfully synthesized *via* double condensation reaction of amine and between amine ( $-NH_2$ ) and mellitic trianhydride (MTA) in polyphosphoric acid (PPA) medium. The strategy to extend conjugated ladder polymer into two-dimension by using the effective condensation reaction have the possibility to utilize rigid ladder polymer with tailored properties for future applications. 2) Synthesis of triphenylene-based covalent triazine networks (sTP-CTNs) in the presence of gaseous catalyst, HCl, *via* solid-state reaction. Compared with conventional synthetic approaches to form triazine-based materials, there are some advantages such as clean and efficient work-up process, solvent-free mild reaction conditions.



## Table of Contents

List of figures.....	iii
List of tables.....	vii
Nomenclature.....	viii
Chapter 1 Design and synthesis of two-dimensional sheet-like BBL structure.....	1
1.1 Abstract.....	1
1.2 Introduction.....	1
1.3 Experimental Section.....	2
1.3.1 Materials.....	2
1.3.2 Instrument.....	2
1.3.3 Preparation of mellitic trianhydride (MTA).....	3
1.3.4 Preparation of 1,2,4,5-tetraaminobenzene (TAB).....	3
1.3.5 Synthesis of 2D-poly(benzoimidazo benzophenanthroline) from 1,2,4,5-tetraaminobenzene (2D-BBL-T).....	3
1.3.6 Synthesis of 2D-poly(benzoimidazo benzophenanthroline) (2D-BBL) from Hexaaminobenzene (2D-BBL-H).....	4
1.3.7 Removal of MnO <sub>4</sub> <sup>-</sup> and selective capturing of dye molecules.....	5
1.4 Results and Discussion.....	6
1.5 Conclusion.....	33
Chapter 2 Solid-state polymerization of hexa-functional nitrile compound.....	34
2.1 Abstract.....	34
2.2 Introduction.....	34
2.3 Experimental Section.....	35
2.3.1 Materials.....	35
2.3.2 Instrument.....	35
2.3.3 Preparation of 2,3,6,7,10,11-hexabromotriphenylene (THBr).....	35
2.3.4 Preparation of triphenylene-2,3,6,7,10,11-hexacarbonitrile (THCN).....	36
2.3.5 Crystallographic data collection and refinement of the structure.....	36



2.3.6 Synthesis of triphenylene-based conjugated triazine networks <i>via</i> solid-state (sTP-CTN) polymerization. ....	36
2.3.7 Synthesis of triphenylene-based conjugated triazine networks with Zinc chloride (Zn-CTN) .....	37
2.4 Results and Discussion .....	37
2.5 Conclusion .....	48
References.....	49
Acknowledgement .....	53

## List of figures

**Figure 1.1.** (a) Solution-state  $^1\text{H}$ -NMR spectrum and (b)  $^{13}\text{C}$ -NMR spectrum of MTA (acetone- $d_6$ ).

**Figure 1.2.** FT-IR (KBr pellet) spectra mellitic trianhydride and mellitic acid precursor.

**Figure 1.3.** (a)  $^1\text{H}$ -NMR spectrum and (b) DIP-MS spectra of TAB.

**Figure 1.4.** (a) Schematic presentation for the formation of 2D-BBL from 1,2,4,5-tetraaminobenzene (TAB) and mellitic anhydride (MA) in polyphosphoric acid (PPA). (b-e) Digital photographs taken during the synthesis of 2D-BBL-T-HT: (b) Tetraaminobenzene (TAB) tetrahydrochloride in PPA at room temperature, (c) after complete dehydrochlorination, the color of media changed from white to orange and transparent. (d) Polymerization with mellitic trianhydride (MTA) at 175 °C. (e) Photograph of as-synthesized 2D-BBL-T-HT. (f) Schematic presentation for the formation of 2D-BBL-H-HT from hexaaminobenzene (HAB) and mellitic anhydride (MA). (g-j) Digital photographs taken during the synthesis of 2D-BBL-H-HT: (g) Hexaaminobenzene (HAB) trihydrochloride in PPA at room temperature. (h) After complete dehydrochlorination, the color of media changed from light brown to red and transparent. (i) Polymerization with mellitic trianhydride (MTA) at 175 °C. (j) Photograph of as-synthesized 2D-BBL-H-HT.

**Figure 1.5.** TGA thermograms of 2D-BBL-T (a) in air; (b) in nitrogen and 2D-BBL-H (c) in air; (d) in nitrogen obtained with the ramping rate of 10 °C min<sup>-1</sup>: In both air and nitrogen atmosphere, all displayed much improved thermal stability, due to the removal of periphery amine ( $-\text{NH}_2$ ) and carboxyl ( $-\text{COOH}$ ) groups.

**Figure 1.6.** TGA thermograms of (a) 2D-BBL-T-HT and (b) 2D-BBL-H-HT with the ramping rate of 10 °C min<sup>-1</sup> in both air and nitrogen condition. Each derivative weight was calculated in nitrogen condition for both polymer. SEM (scale bar: 5  $\mu\text{m}$ ) and TEM (scale bar: 5nm) image of (c-d) 2D-BBL-T-HT and (e-f) 2D-BBL-H-HT.

**Figure 1.7.** SEM images of (a) 2D-BBL-T and (b) 2D-BBL-T-HT; (c) SEM image of 2D-BBL-H-HT and their corresponding carbon, nitrogen and oxygen mapping in that order. Scale bars are 2  $\mu\text{m}$ .

**Figure 1.8.** SEM images of (a) 2D-BBL-H and (b) 2D-BBL-H-HT; (c) SEM image of 2D-BBL-H-HT and their corresponding carbon, nitrogen and oxygen mapping in that order. Scale bars are 2  $\mu\text{m}$ .

**Figure 1.9.** (a) Solution-state  $^{13}\text{C}$ -NMR spectra of MTA (acetone- $d_6$ ) and TAB ( $\text{D}_2\text{O}$ ) and solid-state  $^{13}\text{C}$ -NMR spectra of 2D-BBL-T and after heat treatment, 2D-BBL-T-HT from the region between 220 and 20 ppm. (b) Solution-state  $^{13}\text{C}$ -NMR spectra of MTA (acetone- $d_6$ ). NMR spectra of HAB can not be measured because of sensitivity. Solid-state  $^{13}\text{C}$ -NMR spectra of 2D-BBL-H and after heat treatment, 2D-BBL-H-HT from the region between 220 and 20 ppm.

**Figure 1.10.** (a) Solid-state  $^{13}\text{C}$ -NMR spectra of 2D-BBL-T-HT with 2D-BBL-T and (b) 2D-BBL-H-HT with 2D-BBL-H from the region between 220 and 20 ppm. Inset: unit cell structure of BBL polymers and their corresponding carbon atom. Spinning sidebands are indicated by asterisks. XPS full survey (c) 2D-BBL-T-HT with 2D-BBL-T and (d) 2D-BBL-H-HT with 2D-BBL-H.

**Figure 1.11.** (a) FT-IR full spectra of 2D-BBL-T, 2D-BBL-T-HT, 2D-BBL-H and 2D-BBL-H-HT; (b) PXRD patterns of 2D-BBL-T, 2D-BBL-H and their annealed samples, 2D-BBL-T-HT and 2D-BBL-H-HT.

**Figure 1.12.** Simulated unit cell structure of (a) 2D-BBL-T-HT and (b) 2D-BBL-H-HT (C, grey; N, blue; O, red).

**Figure 1.13.** XPS spectra of 2D-BBL-T: (a) Full survey spectra; High-resolution (b) C 1s, (c) N 1s and (d) O 1s spectra.

**Figure 1.14.** XPS spectra of 2D-BBL-H: (a) Full survey spectra; High-resolution (b) C 1s, (c) N 1s and (d) O 1s spectra.

**Figure 1.15.** XPS spectra of 2D-BBL-T-HT: (a) Full survey spectra; High-resolution (b) C 1s, (c) N 1s and (d) O 1s spectra.

**Figure 1.16.** XPS spectra of 2D-BBL-H-HT: (a) Full survey spectra; High-resolution (b) C 1s, (c) N 1s and (d) O 1s spectra.

**Figure 1.17.** Permanent porosities of 2D-BBL-T-HT (red) and 2D-BBL-H-HT (blue). (a) Nitrogen adsorption (open circles) and desorption (filled circles) isotherms at 77 K. Inset: pore size distribution calculated from NLDFT. (b)  $\text{CO}_2$  adsorption-desorption isotherms at 273 K. Inset:  $Q_{st}$  for  $\text{CO}_2$  as a function of gas uptake estimated from low-pressure isotherms at 273 K and 298K. (c)  $\text{H}_2$  adsorption-desorption isotherms at 77 K. Inset:  $Q_{st}$  for  $\text{H}_2$  as a function of gas uptake estimated from low-pressure isotherms at 77 K and 87 K.

**Figure 1.18.** BET plot of (a) 2D-BBL-T-HT and (b) 2D-BBL-H-HT at 77 K using nitrogen as adsorbate.

**Figure 1.19.** Permanent porosities of 2D-BBL-T-HT: (a) H<sub>2</sub> adsorption-desorption isotherms at 77 K and 87 K; (b) CO<sub>2</sub> adsorption-desorption isotherms at 273 K and 298 K. Permanent porosities of 2D-BBL-H-HT; (c) H<sub>2</sub> adsorption-desorption isotherms at 77 K and 87 K; (d) CO<sub>2</sub> adsorption-desorption isotherms at 273 K and 298 K.

**Figure 1.20.** UV-vis spectra of (a) MnO<sub>4</sub><sup>-</sup>, (b) Methylene blue and (c) Methyl orange aqueous solution in the presence of 2D-BBL-T-HT (red line) and 2D-BBL-H-HT (blue line) for 5 min. (d) UV-vis spectra of MB/MO aqueous solution in the presence of 2D-BBL-T-HT for 5 min. (e) Comparison of the dye adsorption ability of 2D-BBL-T-HT (red) and 2D-BBL-H-HT (Blue). Digital photographs of (f) dye adsorption test by using 2D-BBL-T-HT and (g) 5mg of 2D-BBL-T-HT equipped filter.

**Figure 2.1.** (a) Electron ionized mass spectroscopy of TPBr, which is 701.8 m/z (M<sup>+</sup>, Calcd. 701.5) and debromination occur during measurement which show at 621.8 and 541.8 m/z peaks by strong electron source. (b) Electron ionized mass spectroscopy of TPCN, which is 378.1 m/z (M<sup>+</sup>, Calcd. 378.1). (c) <sup>1</sup>H-NMR and (d) <sup>13</sup>C-NMR spectra of triphenylene-2,3,6,7,10,11-hexacarboxylic acid (acetone-d<sub>6</sub>).

**Figure 2.2.** (a) Ball and stick packing diagram of THCN crystal viewed along the crystallographic z-axis. (b) Diagram of THCN red lines indicate interdigitation between three nitrile functional groups which reaction occur. (color code: grey=carbon; blue=nitrogen; white=hydrogen). (c) Powdered and single crystal X-ray diffraction (XRD) pattern of THCN.

**Figure 2.3.** TGA thermograms of THCN crystals with ramping rate of 10 °C min<sup>-1</sup>: (a) in nitrogen and (b) in air.

**Figure 2.4.** Synthesis of triphenylene-based conjugated triazine network polymer via solid-state polymerization of THCN (sTP-CTN). (a) Schematic representation of sTP-CTN formation in the presence of hydrochloric acid gas. Digital photographs of (b) THCN crystals and (c) after synthesis of CTN-0 at 450 °C. SEM image of (d-e) CTN-0 at different scale. (Scale bar: 50 μm and 2 μm.) (f) Solid <sup>13</sup>C NMR spectrum of CTN-0.

**Figure 2.5.** (a-b) Optical microscopy images of THCN crystals. (c-d) SEM images of CTN-0.

**Figure 2.6.** (a) A digital photograph of Zn-CTN. (b-d) SEM images of Zn-CTN. (e) SEM energy-dispersive X-ray (EDS) spectrum of Zn-CTNs, showing corresponding the contents of element (wt.%).

**Figure 2.7.** (a) Fourier transform infrared spectroscopy (FT-IR) spectra of precursor, HTCN and two sTP-CTNs (KBr pellets). The s-triazine of sTP-CTNs vibrated at both 1519 and 1380  $\text{cm}^{-1}$ . (b) X-ray diffraction (XRD) patterns of CTN-0 and Zn-CTN.

**Figure 2.8.** XPS spectra of CTN-0: (a) Full survey spectra; High-resolution (b) C 1s, (c) N 1s and (d) O 1s spectra.

**Figure 2.9** TGA thermograms of CTN-0 crystals with ramping rate of 10  $^{\circ}\text{C min}^{-1}$ : (a) in air and (b) in nitrogen.

**Figure 2.10.** TGA thermograms of Zn-CTN with ramping rate of 10  $^{\circ}\text{C min}^{-1}$  in air.

## List of tables

**Table 1.1.** Elemental analysis of purified TAB.

**Table 1.2.** Elemental compositions of 2D-BBL-H and 2D-BBL-H-HT.

**Table 1.3.** Elemental compositions of 2D-BBL-H and 2D-BBL-H-HT.

**Table 2.1.** Crystallographic data for THCN.

**Table 2.2.** Elemental compositions of THCN crystals and sTP-CTN.

## Nomenclature

---

<b>BBL polymer</b>	Poly(benzoimidazobenzophenanthroline) ladder polymer
<b>2D</b>	Two-dimensional
<b>MTA</b>	Mellitic trianhydride
<b>PPA</b>	Polyphosphoric acid
<b>BET</b>	Brunauer–Emmett–Teller
<b>NLDFT</b>	Nonlocal density functional theory
<b>MOFs</b>	Metal-organic frameworks
<b>PCPs</b>	Porous coordination polymers
<b>COFs</b>	Covalent-organic frameworks
<b>PONs</b>	Porous organic networks
<b>2D-BBL</b>	Two-dimensional BBL (2D-BBL) networks
<b>TAB</b>	1,2,4,5-Tetraaminobenzene
<b>HAB</b>	Hexaaminobenzene
<b>FE-SEM</b>	Field emission scanning electron microscopy
<b>TGA</b>	Themogravimetric analysis
<b>XPS</b>	X-ray photoelectron spectroscopy
<b>EA</b>	Elemental analysis
<b>XRD</b>	X-Ray diffraction
<b>FT-IR</b>	Fourier transformation infrared spectroscopy
<b>HR-TEM</b>	High-resolution transmission electron microscopy
<b>MB</b>	Methylene blue
<b>MO</b>	Methyl orange
<b>THBr</b>	2,3,6,7,10,11-hexabromotriphenylene
<b>THCN</b>	Triphenylene-2,3,6,7,10,11-hexacarbonitrile
<b>HCl</b>	Hydrochloric acid
<b>sTP-CTN</b>	Triphenylene-based conjugated triazine networks
<b>DMF</b>	<i>N,N</i> -Dimethylformamide
<b>EDXS</b>	Energy-dispersive X-ray spectroscopy

---

## Chapter 1 Design and synthesis of two-dimensional sheet-like BBL structure.

### | Abstract

Linear poly(benzimidazobenzophenanthroline) ladder like (BBL) polymers attracted high interest because of their outstanding properties such as thermal and chemical stability, electrical conductivity, optical and electronic properties, etc. Nevertheless, two-dimensional (2D) BBL polymers have not been reported up to now. Here, we introduce 2D sheet-like BBL structures *via* polycondensation of mellitic anhydride (MTA) with di- and tri-functional aromatic amines (M2, M3) in polyphosphoric acid (PPA) medium. These unique 2D BBLs are constructed with strong fused aromatic ring and exhibit permanent microporosity with a high Brunauer–Emmett–Teller (BET) surface area of 611 m<sup>2</sup> g<sup>-1</sup> for 2D-BBL-T-HT (M2) and 365 m<sup>2</sup> g<sup>-1</sup> for the 2D-BBL-H-HT (M3) with different pore diameter. 2D BBLs show experimentally that increasing hydrogen uptake as decreasing pore diameter in porous network. At low pressure, the 2D-BBL-H-HT show higher hydrogen (H<sub>2</sub>) (1.65 wt.% at 273 K and 1 bar) and carbon dioxide (CO<sub>2</sub>) (15.6 wt.% at 273 K and 1 bar) uptake capacities than 2D-BBL-T-HT. These findings represent a major significance in the synthesis and application of 2D BBL network structures.

### | Introduction

Design, synthesis and application of advanced new multi-dimensional materials arouse huge interests from the inorganic materials, e.g., zeolites<sup>1-2</sup> and silica, to hybrid material such as metal-organic frameworks (MOFs)<sup>3</sup>, porous coordination polymer (PCPs)<sup>4</sup>, pure organic networks of covalent-organic frameworks (COFs)<sup>5</sup>, porous cages<sup>6-7</sup> and porous organic networks (PONs)<sup>8-9</sup>. Among them, two-dimensional porous network polymer has undergone evolution since they possess light weight, high surface area, permanent porosity, high thermal and chemical stability<sup>10-12</sup>. Finely controllable structure which provides potential for various applications such as electronics, energy conversion and storage, catalysts, gas separation and storage and molecular sensing<sup>13-14</sup>.

The benzimidazo-benzophenanthroline conjugated ladder-type (BBL) polymer was firstly introduced in the 1960s by R.L. Van Deusen et al.,<sup>15</sup> since then, many different conjugated BBL aromatic linear polymers have been synthesized and studied<sup>16-17</sup>. Fully conjugated ladder type polymer is connected and fused with multiple strands of covalent network of monomers with ordered bonding, planar and rigid backbones<sup>18-19</sup>. Direct polycondensation of multifunctional monomers and zip-up flexible polymer and generate a long range of polyheteroaromatic ladder type BBL networks which have large  $\pi$ -conjugated system with plenty of nitrogen and oxygen atoms in extended skeleton. It is well-known that the structures with extended  $\pi$ -electron conjugation display exceptional physical



properties such as excellent thermal, chemical and mechanical stability, optical and electronic properties<sup>19-21</sup>. Therefore, these structures have been intensively investigated advanced applications such as photovoltaic assemblies<sup>22-24</sup>, photodetectors<sup>25</sup>, capacitors<sup>26-27</sup>, optoelectronic devices<sup>28-29</sup>, and field-effect transistor assemblies<sup>30-31</sup>. In contrast, very little is currently explored regarding gas adsorption and storage ability due to highly rigidity and extremely dense packing<sup>32</sup>. Here, we designed and synthesized two-dimensional BBL (2D-BBL) network by using two different monomers, 1,2,4,5-tetraaminobenzene (TAB) and hexaaminobenzene (HAB) which construct 2D-BBL-T and 2D-BBL-H respectively. Conjugated sheet-like ladder BBLs are planar structure and carry huge advantage over its linear BBL analogue in terms of large surface area, heavily introduced functionalities, permanent microporosity and extended heteroatom containing skeleton. 2D BBLs have constructed with the same chemical bonding and show similar characteristics but difference in a hole dimension plays an important role of increasing gas adsorption ability. In this approach, 2D-BBL-T-HT and 2D-BBL-H-HT designed and realized to possess different pore diameters (1.5 and 1.0 nm) to investigate impact of pore size on gas adsorption and/or storage applications and size-selective capture for organic dye molecules.

## | Experimental Section

### 1.3.1 Materials

All solvents and reagent for synthesis were commercially available and used without further purification, unless otherwise specified. Pd/C 10% (75990), Polyphosphoric acid (208213), 37% HCl (258138) were purchased from Aldrich Chemical Inc. Celite 545 (C03440) was provided by Samchun Pure Chemical Co., LTD. 1,2,4,5-Tetraaminobenzene (TAB) and Hexaaminobenzene (HAB) was prepared according to the literature.<sup>28, 33</sup>

### 1.3.2 Instrument

The field emission scanning electron microscopy (FE-SEM) was performed on FEI Nanonova 230 (USA). Thermogravimetric analysis (TGA) was conducted on a PerkinElmer STA 8000 at a heating rate of 10 °C min<sup>-1</sup> under air or nitrogen. The specific surface area was measured by nitrogen adsorption-desorption isotherms using the Brunauer-Emmett-Teller (BET) method on BELSORP-max (Japan BEL Co., Ltd., Japan). X-ray photoelectron spectra (XPS) were recorded on a Thermo Fisher K-alpha XPS spectrometer. Elemental analysis (EA) was conducted with Thermo Scientific Flash 2000. X-Ray diffraction (XRD) patterns were recorded with a Rigaku D/MAZX 2500V/PC with Cu-K $\alpha$  radiation (40 kV, 20 mA,  $\lambda = 1.5418 \text{ \AA}$ ). Fourier transformation infrared (FT-IR) spectra were obtained by PerkinElmer Spectrum 100 using KBr

pellets.  $^1\text{H}$ -NMR and  $^{13}\text{C}$ -NMR were obtained on a 400 MHz FT-NMR AVANCE III HD (Bruker, USA) spectrometer. Solid Carbon NMR were recorded on a 600 MHz FT-NMR VNMRS 600 (Varian, USA) spectrometer. The high-resolution transmission electron microscopy (HR-TEM) was performed on JEOL JEM-2100F microscope. The TEM specimen were prepared by dipping carbon micro-grids (Ted Pella Inc., 200 Mesh Copper Grid) into well-dispersed samples in ethanol. UV-vis NIR spectrophotometer (Agilent Technologies, CA, USA) was used to record the dye adsorption ability.

### 1.3.3 Preparation of mellitic trianhydride (MTA)

In the Pyrex tube, well-ground mellitic acid (0.5 g, 1.46 mmol) and 3 mL of acetyl chloride was charged, and the tube was flame-sealed and the mixture was heated at 120 °C for 20 h with good stirring. The white precipitate was separated from the light-brown solution. The resultant white precipitate was filtered and washed with benzene three times to purify, and then vacuum dried in desiccator in the presence  $\text{P}_2\text{O}_5$  at room temperature (R. T), overnight. Final product was white small crystals to afford 0.40 g (95.7%) and was used without further purification.  $^1\text{H}$ -NMR (Acetone- $d_6$ , 400 MHz) no peaks were observed as there are no protons;

### 1.3.4 Preparation of 1,2,4,5-tetraaminobenzene (TAB)

In a high-pressure hydrogenation reaction bottle, 1,3-diamino-4,6-dinitrobenzene (DADNB) (5.0 g, 0.025 mol) and 10% Pd/C (0.67 g) were placed with 300 mL of 5 v/v% hydrochloric acid. The reaction flask was placed tightly in hydrogenation reaction apparatus and charging with hydrogen gas ( $\text{H}_2$ , 5 bar) for 5 days. The orange color of DADNB was disappeared when reaction finished and become transparent dark green solution. The resultant solution was passed through celite with conc. HCl solution (37% HCl) in the receiving Erlenmeyer flask. The obtained white crystals in the receiving flask were collected by filtration and again washed with 37% HCl and ether to give 6.60 g (92.1% yield) of TAB.  $^1\text{H}$ -NMR (DMSO- $d_6$ , 400MHz)  $\delta$  = 7.71 (2H, s), 6.83 (4H, s); MS (DIP-MS).  $m/z$  (%) = 138 (100) [ $\text{M}^+$ ]. Anal. Calcd. (%) for  $\text{C}_6\text{H}_{14}\text{Cl}_4\text{N}_4$  (Mol. wt.%): C, 25.37; H, 4.97; Cl, 49.93; N, 19.73. Found: C, 25.39; H, 4.87; Cl, 50.73 (Calcd.); N, 19.01.

### 1.3.5 Synthesis of 2D-poly(benzoimidazo benzophenanthroline) from 1,2,4,5-tetraaminobenzene (2D-BBL-T)

Two-dimensional poly(benzoimidazo benzophenanthroline) (2D-BBL-T) was synthesized by powerful condensation reaction between 1,2,4,5-tetraaminobenzene (TAB) and mellitic trianhydride (MTA) in polyphosphoric acid (PPA). TAB (2.00 g, 7.23 mmol) and PPA (90.0 g, 115% P<sub>2</sub>O<sub>5</sub> assay) were charged in flask and stirred by using a high-torque mechanical stirrer at room temperature under nitrogen atmosphere. The temperature was stepwise increased to 60 °C (30 °C and 40 °C for 1 d; 50 °C for 5 d; 60 °C for 1 d), to completely remove HCl in the TAB. After complete removal of HCl gas the transparent and orange color media was cooled down to room temperature and MTA (1.35 g, 4.69 mmol) was added at room temperature. Then, the temperature was maintained at 30 °C for 24 h for homogeneous mixing and slowly increased to 100 °C, again increased to 150 °C for 12 h to form precursor of ring closure BBL polymer. Ring closure occurs, and high viscous gel-like mixture was achieved after raising the temperature to 175 °C for 6 h. The reaction mixture became dark and started sticking to mechanical stirrer rod due to the formation of high molecular weight polymer. The deep brown solid was collected and washed by Soxhlet extraction with water to remove residual PPA and methanol to get rid of unreacted monomer for two days each as well as small molecular impurities, if any. The product was washed with water again and freeze-dried at -120 °C under reduced pressure (~10<sup>-5</sup> Torr) to afford 1.74 g (95.6% yield).

### **1.3.6 Synthesis of 2D-poly(benzoimidazo benzophenanthroline) (2D-BBL) from hexaaminobenzene (2D-BBL-H)**

Two-dimensional poly(benzoimidazo benzophenanthroline) (2D-BBL-H) was synthesized from triple condensation reaction between hexaaminobenzene trihydrochloride (HAB) and mellitic trianhydride (MTA) in polyphosphoric acid (PPA). HAB (1.00 g, 3.60 mmol) and PPA (30.0 g, 115% P<sub>2</sub>O<sub>5</sub> assay) were placed in flask and stirred by using a high-torque mechanical stirrer at room temperature under nitrogen atmosphere. The temperature was stepwise increased to 60 °C (30 °C and 40 °C for 1 d; 50 °C for 5 d and 60 °C for 1 d), to completely remove HCl in the HAB molecule. The reddish and transparent mixture was cooled down to room temperature and MTA (1.04 g, 3.60 mmol) was added at room temperature. Then, the temperature was maintained at 30 °C for 24 h for homogeneous mixing and slowly increased to 100 °C, again increased to 150 °C for 12 h to form precursor of ring closure BBL polymer. As ring closer reaction occurred, high viscous gel-like mixture was achieved after increasing the temperature to 175 °C for 6 h. The black solid was collected and washed by Soxhlet extraction with water to remove residual PPA and methanol to get rid of unreacted monomer for two days each as well as small molecular impurities, if any. The product was washed with water again and freeze-dried at -120 °C under reduced pressure (~10<sup>-5</sup> Torr) to afford 1.17 g (93.03% yield).

### 1.3.7 Removal of $\text{MnO}_4^-$ and selective capturing of dye molecules

A 3 mL of aqueous solution of  $\text{KMnO}_4$  (0.25 mM) was added to a small vial with the presence of each 2D-BBLs (5 mg of 2D-BBL-T-HT and 1 mg of 2D-BBL-H-HT). After few shakes for 5 min, the mixture was filtered at 0.45  $\mu\text{m}$  membrane filter, and then filtrate was analyzed by UV-vis spectrometer to determine removal efficiency. For the adsorption of dyes, 0.01 mM of methylene blue (MB) and methyl orange (MO) was prepared. 2D-BBLs (5 mg of 2D-BBL-T-HT and 1 mg of 2D-BBL-H-HT) was added into the solution and mixed by simple shaking for 5 min. A 3 mL of MB/MO mixture (v/v, 1:1 with the same concentration of 0.01 mM) was used for the selectivity test.

Results and Discussion

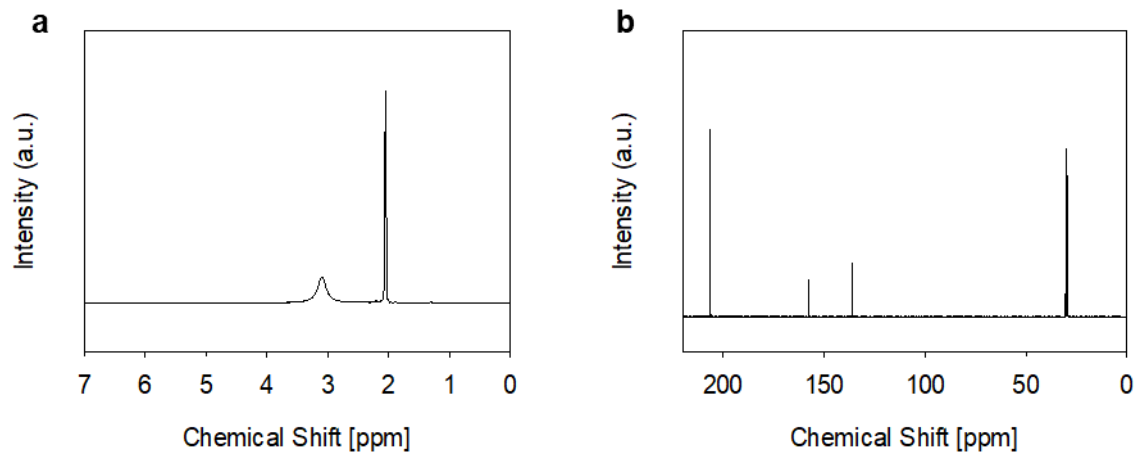


Figure 1.1. (a) Solution-state <sup>1</sup>H-NMR spectrum and (b) <sup>13</sup>C-NMR spectrum of MTA (acetone-d<sub>6</sub>).

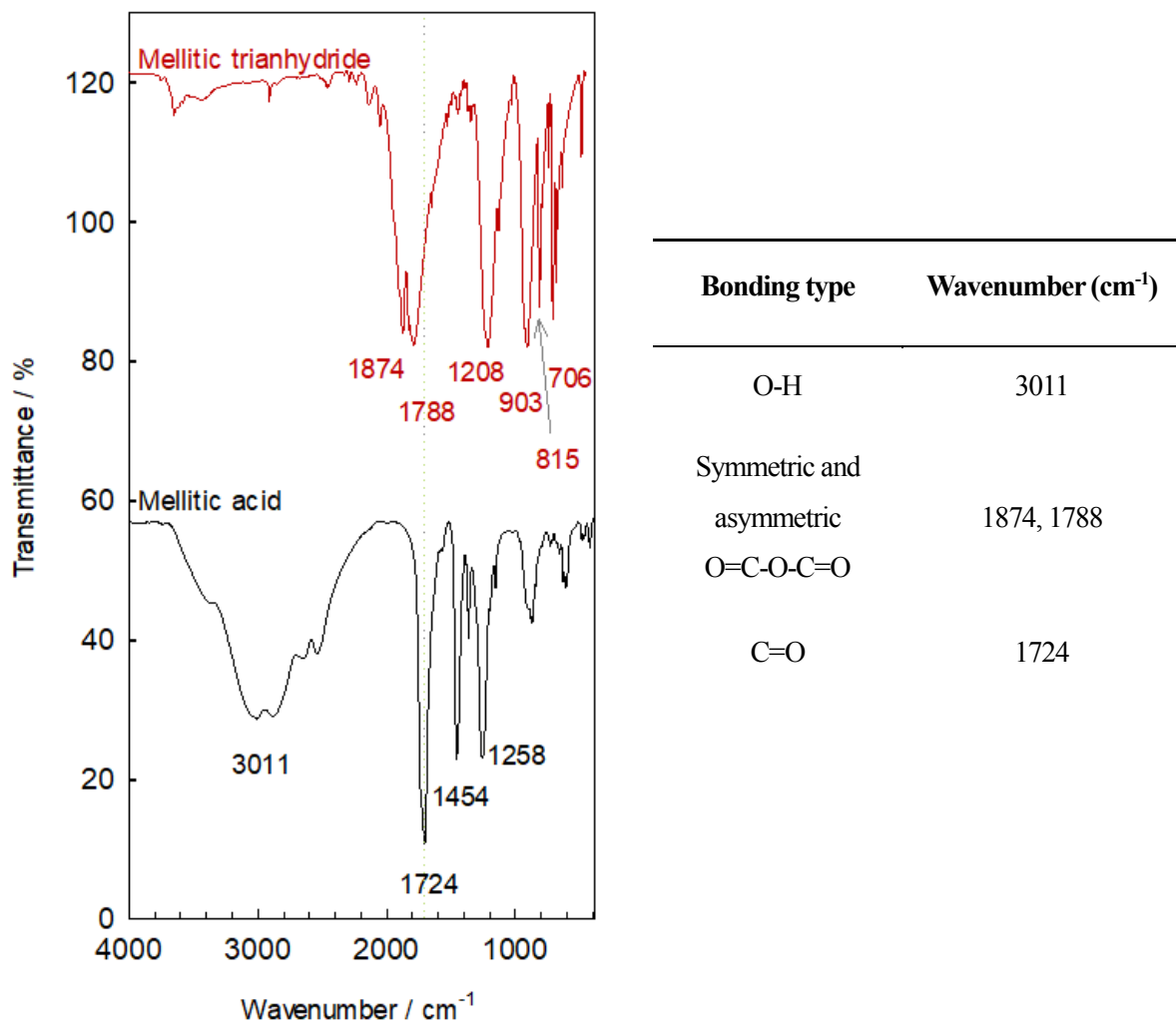
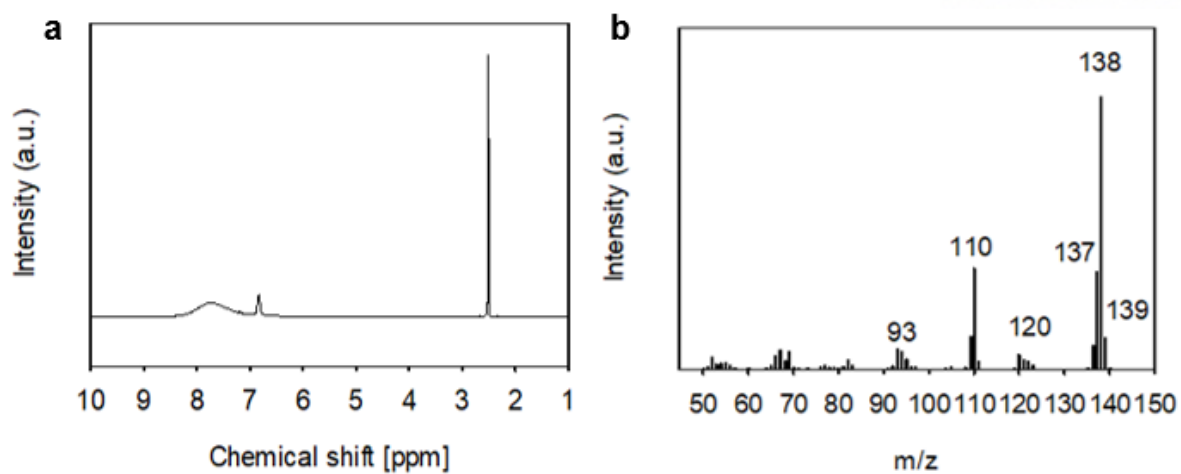


Figure 1.2. FT-IR (KBr pellet) spectra mellitic trianhydride and mellitic acid precursor.



**Figure 1.3.** (a) <sup>1</sup>H-NMR spectrum and (b) DIP-MS spectra of TAB.

**Table 1.1.** Elemental analysis of purified TAB.

Element	C	N	H	Cl	Sum
Cal. (wt.%)	25.37	19.73	4.97	49.93	100
Found	25.39	19.01	4.87	50.73 <sup>a</sup>	100

<sup>a</sup> Quantitative value of 1,2,4,5-tetraaminobenzene tetrahydrochloride.

As shown in figure 1.4, holey two-dimensional poly(benzimidazo-benzophenanthroline) conjugated ladder-type polymers (2D-BBL) were synthesized by condensation reaction between mellitic trianhydride (MTA) with two different amines, tetraaminobenzene (TAB) and hexaaminobenzene (HAB), respectively. TAB and HAB were converted to salt form with dry hydrochloric acid (HCl) to stabilize, which protects amino group against oxidation. Each amine salt was placed in polyphosphoric acid (PPA) solution and stirred by using a high-torque mechanical stirrer at lower temperature (below 60 °C) under nitrogen condition. HCl molecules were continuously removed and free TAB and HAB amines were obtained and showed clear and transparent orange and red color which means perfect removal of HCl molecules. (Figure 1.4c and 1.4h). Then, free amine was reacted with MTA monomers at 150 °C for building up amide form first and further heated at 175 °C for complete cyclization (Scheme 1.1). Both polymers were homogeneously mixed and dehydrated in PPA which act as both solvents and catalysts. Double condensation reaction between amines and carboxyl groups give high viscous polymer consisted of TAB (2D-BBL-T) and HAB (2D-BBL-H). After completion of the reaction, the resulting gel-like material was poured into deionized water (D.I. water) and obtained dark, brown powder by filtration (Figure 1.4e and 1.4j). The precipitates were worked-up with D.I. water and methanol by Soxhlet extraction for 3 days each to get rid of low molar mass impurities and PPA. Final products, 2D-BBL-T and 2D-BBL-H were freeze-dried at -120 °C under reduced pressure ( $\sim 10^{-5}$  Torr). The expected 2D-BBL-T and -H structures have similar structures, fully aromatized backbones, merged benzene ring and five-membered ring with nitrogen atoms and one ketone but different numbers of functional group and hole size (2.1 nm and 1.0 nm) which can influence the physical and chemical properties of the framework.

To understand the removal of undesired edge functional groups, small molecules which adsorbed inside of the polymers and reach complete cyclization, 2D-BBL-T and 2D-BBL-H were subjected to thermogravimetric analysis (TGA) under nitrogen and air condition. Both polymer showed stepwise weight loss and significant weight derivative changes up to 200 °C due to the removal of trapped small impurities such as moisture (Figure 1.5). The gradual weight loss occurred in the temperature range of 200-330 °C was associated with removal of amine and carboxylic groups at the edges of 2D-BBL-T and 2D-BBL-H (Figure 1.4a and 1.4f)<sup>34-36</sup>. 2D-BBL-T and 2D-BBL-H showed high thermal stability up to 500 °C and started to decompose framework structure (Figure 1.5). Therefore, 2D-BBL-T and 2D-BBL-H were thermally annealed at 450 °C and obtained heat treated samples 2D-BBL-T-HT and 2D-BBL-H-HT, respectively (Figure 1.6a and 1.6b). After heat treatment, the color of the samples was changed to dark black confirmed extension of conjugation for enhanced electron conductivity. TGA results of 2D-BBL-T-HT and 2D-BBL-H-HT showed that polymer physically adsorbed moisture in air even heat treatment and all displayed much improved thermal stability due to the removal of periphery amine ( $-NH_2$ ) and carboxyl ( $-COOH$ ) groups (Figure 1.6a and 1.6b)<sup>37</sup>.

Before and after heat treatment, the visual appearance 2D-BBL-T and 2D-BBL-H were

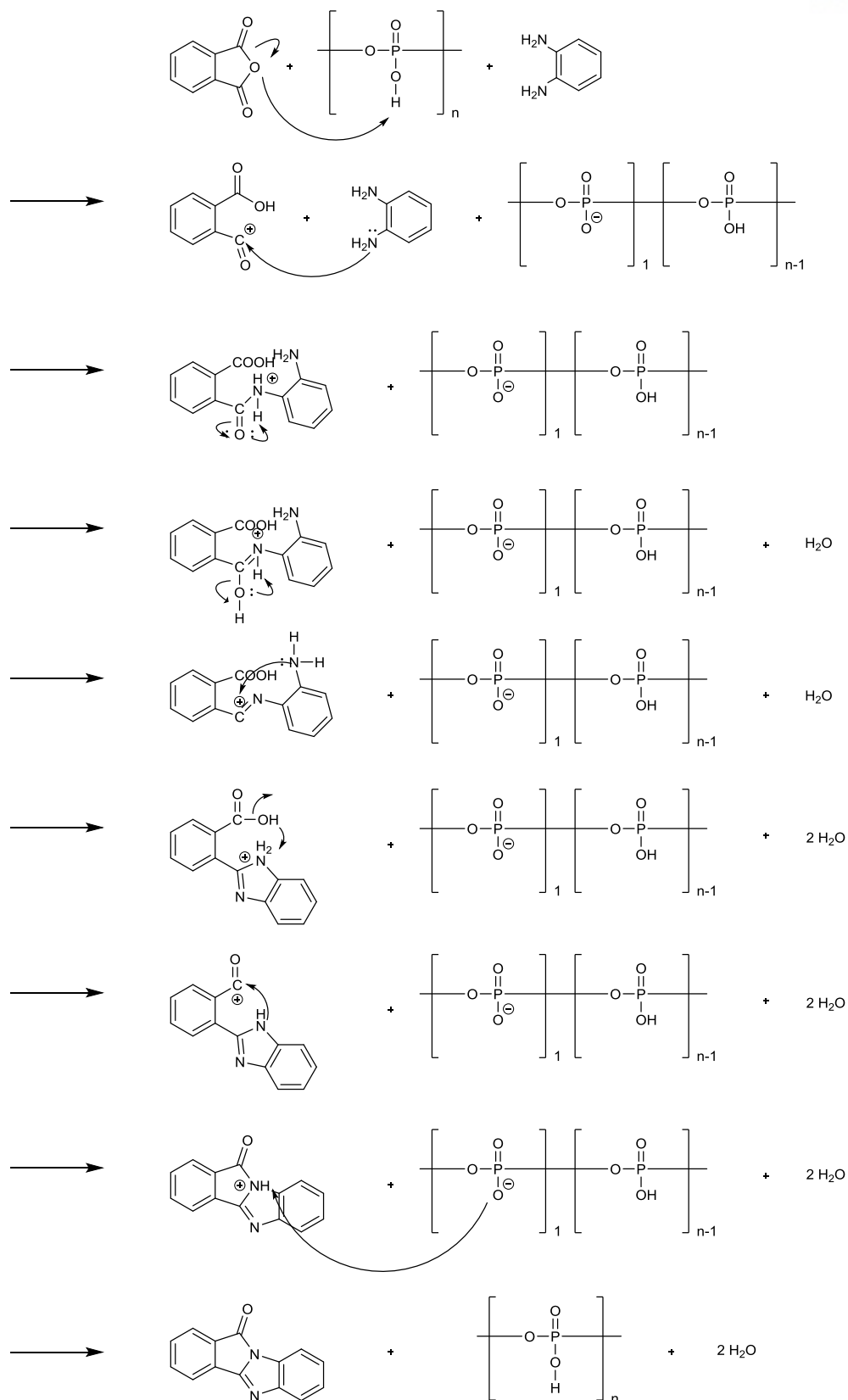
similar surface morphology which indicates their skeleton is thermally stable up to 450 °C (Figure 1.6c-f, 1.7 and 1.8). FE-SEM and TEM images of 2D-BBL-T-HT and 2D-BBL-H-HT displayed few micron grain size and they have coral-like shape with stacked layer and large accessible space. SEM elemental mapping images clearly illustrate a homogeneous distribution of carbon (red), nitrogen (green) and oxygen (cyan) atoms in 2D-BBL-T-HT and 2D-BBL-H-HT (Figure 1.7c and 1.8c).





**Figure 1.4.** (a) Schematic presentation for the formation of 2D-BBL from 1,2,4,5-tetraaminobenzene (TAB) and mellitic anhydride (MA) in polyphosphoric acid (PPA). (b-e) Digital photographs taken during the synthesis of 2D-BBL-T-HT: (b) Tetraaminobenzene (TAB) tetrahydrochloride in PPA at room temperature, (c) after complete dehydrochlorination, the color of media changed from white to orange and transparent. (d) Polymerization with mellitic trianhydride (MTA) at 175 °C. (e) Photograph of as-synthesized 2D-BBL-T-HT. (f) Schematic presentation for the formation of 2D-BBL-H-HT from

hexaaminobenzene (HAB) and mellitic anhydride (MA). (g-j) Digital photographs taken during the synthesis of 2D-BBL-H-HT: (g) Hexaaminobenzene (HAB) trihydrochloride in PPA at room temperature. (h) After complete dehydrochlorination, the color of media changed from light brown to red and transparent. (i) Polymerization with mellitic trianhydride (MTA) at 175 °C. (j) Photograph of as-synthesized 2D-BBL-H-HT.



**Scheme 1.1.** The condensation mechanism for the formation of benzimidazo-benzophenanthroline compounds rings in polyphosphoric acid (PPA), which is acid catalysts for dehydration as well as solvent for polymerization.

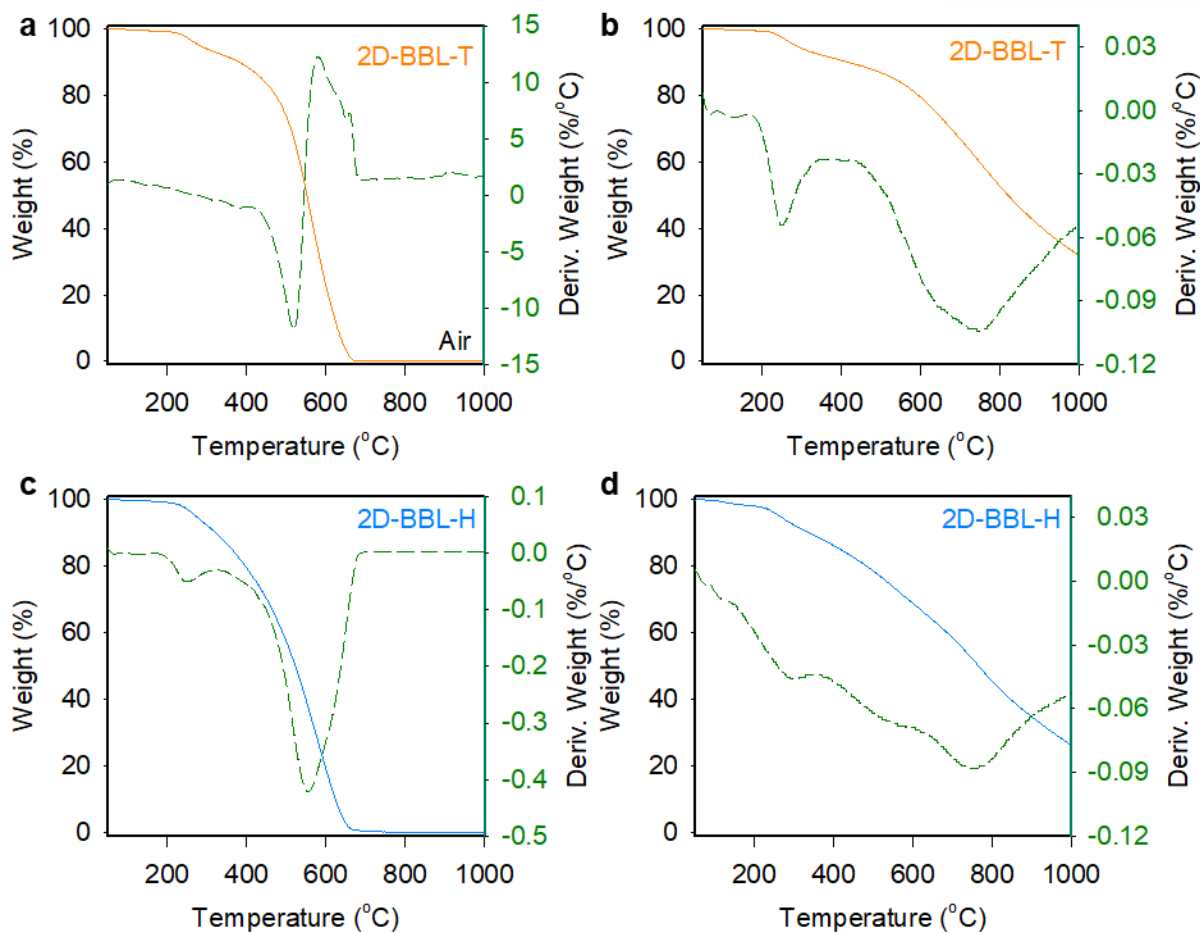


**Figure 1.5.** TGA thermograms of 2D-BBL-T (a) in air; (b) in nitrogen and 2D-BBL-H (c) in air; (d) in nitrogen obtained with the ramping rate of  $10\text{ }^{\circ}\text{C min}^{-1}$ : In both air and nitrogen atmosphere, all displayed much improved thermal stability, due to the removal of periphery amine ( $-\text{NH}_2$ ) and carboxyl ( $-\text{COOH}$ ) groups.

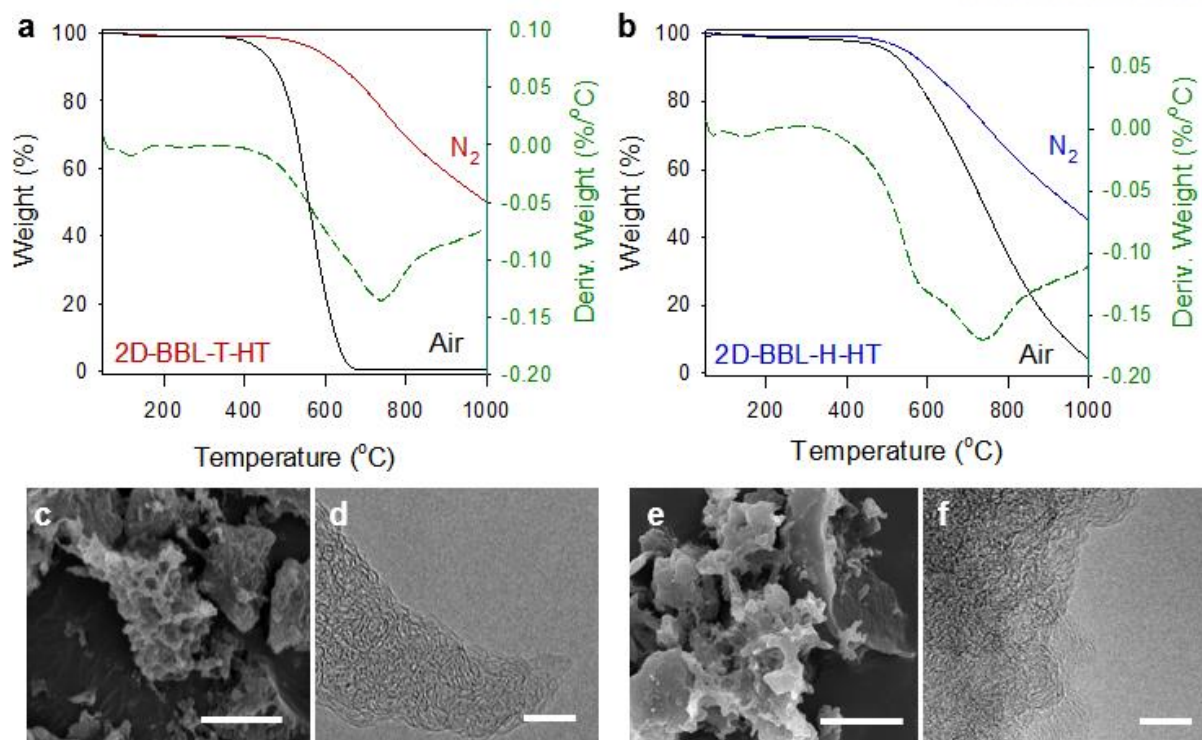


**Figure 1.6.** TGA thermograms of (a) 2D-BBL-T-HT and (b) 2D-BBL-H-HT with the ramping rate of  $10\text{ }^{\circ}\text{C min}^{-1}$  in both air and nitrogen condition. Each derivative weight was calculated in nitrogen condition for both polymer. SEM (scale bar:  $5\text{ }\mu\text{m}$ ) and TEM (scale bar:  $5\text{ nm}$ ) image of (c-d) 2D-BBL-T-HT and (e-f) 2D-BBL-H-HT.



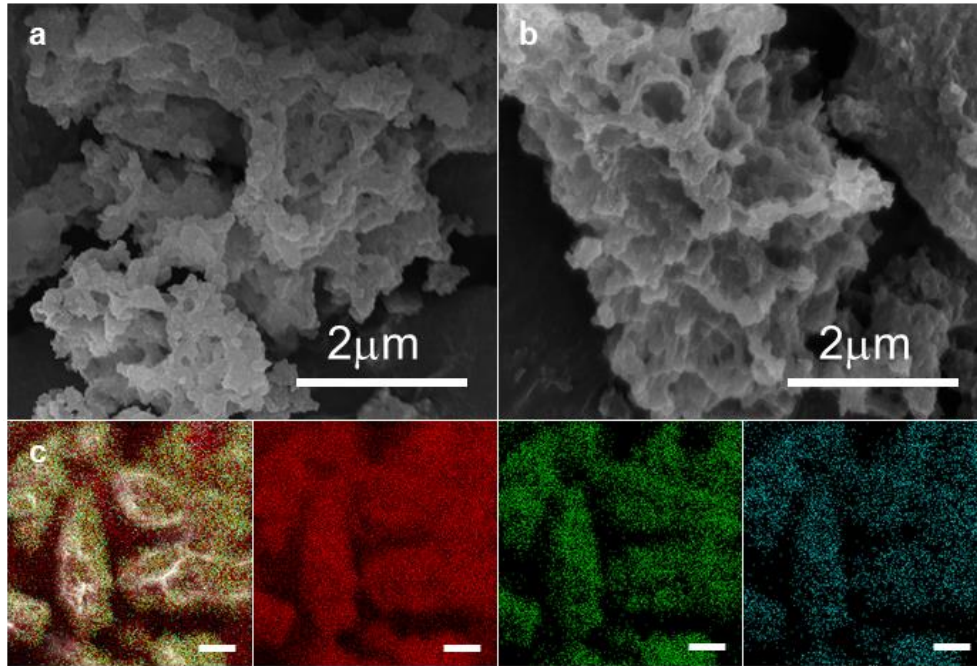


**Figure 1.7.** SEM images of (a) 2D-BBL-T and (b) 2D-BBL-T-HT; (c) SEM image of 2D-BBL-H-HT and their corresponding carbon, nitrogen and oxygen mapping in that order. Scale bars are 2  $\mu\text{m}$ .

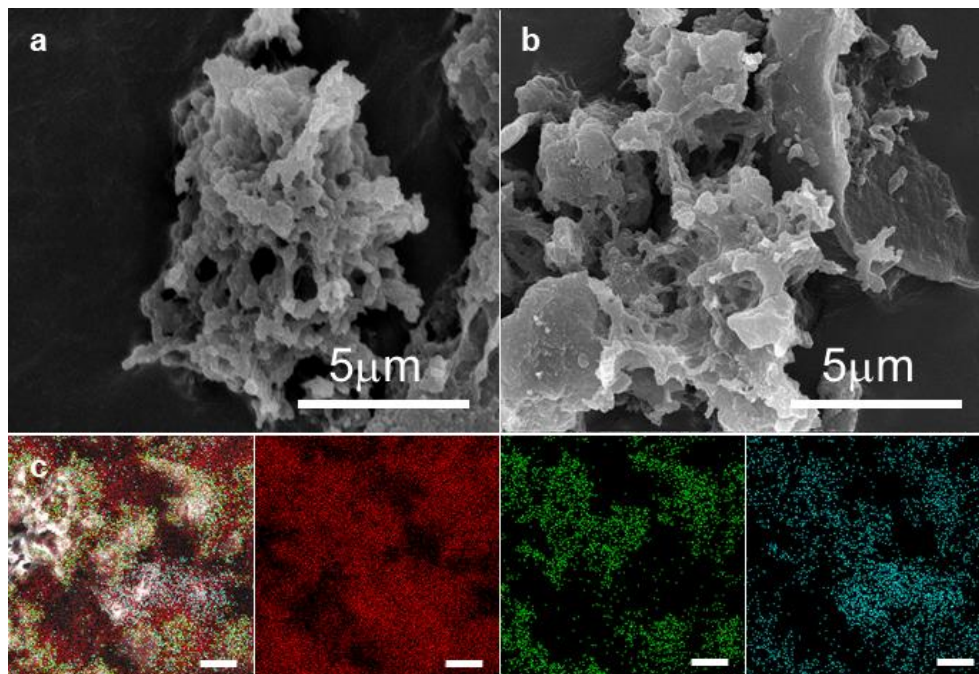


**Figure 1.8.** SEM images of (a) 2D-BBL-H and (b) 2D-BBL-H-HT; (c) SEM image of 2D-BBL-H-HT and their corresponding carbon, nitrogen and oxygen mapping in that order. Scale bars are 2  $\mu\text{m}$ .

As depicted in Figure 1.9, we performed the  $^{13}\text{C}$  magic-angle spinning (MAS) NMR measurements and compared the former to the  $^{13}\text{C}$  spectrum of precursor. 2D-BBL-T and 2D-BBL-T-HT shows identical five well resolved signal at 162, 142, 134, 124 and 93 ppm. The peak at 162 ppm is assigned to the carbon in ketone and unambiguously decreased after heat treatment due to further cyclization and removal of functional groups in periphery. In case of 2D-BBL-H and 2D-BBL-H-HT, four signals at 166, 142, 135 and 119 ppm were good agreement with the proposed structures (Figure 1.10a and 1.10b).

Fourier-transform infrared spectroscopy (FT-IR) and X-ray photon electron spectroscopy (XPS) were performed to confirm the chemical connectivity and formation of benzimidazole ring and pyrrolidinone moiety. In FT-IR spectra were consistent with the proposed structures 2D BBL structure<sup>38</sup>. Also, no significant changes were observed even after heat treatment which means that polymer skeleton is stable over 450 °C (Figure 1.11a). The peaks at 1746  $\text{cm}^{-1}$  and 1719  $\text{cm}^{-1}$  were assigned to the C=O stretching vibration band of introduced ketone functional groups and the peaks at 1616  $\text{cm}^{-1}$  and 1612  $\text{cm}^{-1}$  are C=N stretching absorption in 2D-BBL-T-HT and 2D-BBL-H-HT. The absorption at 1266  $\text{cm}^{-1}$  and 1260  $\text{cm}^{-1}$  were assigned to the C-N stretching vibration band of the cyclic tertiary amine structure<sup>15</sup>. Before heat treatment, small shoulder peak around 1780  $\text{cm}^{-1}$  appear due to the incomplete cyclization but heat treatment induced further reaction and the peak disappeared as we intended<sup>38</sup>. The peak at 3376  $\text{cm}^{-1}$  (2D-BBL-T-HT) and 3369  $\text{cm}^{-1}$  (2D-BBL-H-HT) were broaden due to overlap of free N-H stretching at the edges, hydroxyl group (-OH) from trapped moisture and polymeric hydrogen bonding.

XRD diffraction patterns showed broad [002] peak of 2D-BBL-T and 2D-BBL-T-HT appeared at 22.8° and 23.7° (corresponding to the layer-to-layer distance of 3.94 Å and 3.75 Å) (Figure 1.11b). In case of 2D-BBL-H and 2D-BBL-H-HT, [002] peaks shifted in higher degree, 25.3° and 25.7° which are corresponding to the layer-to-layer distance of 3.51 Å and 3.51 Å. The inter hole distance of 2D-BBL-T and 2D-BBL-H was expected to be 2.1 nm and 1.0 nm respectively (Figure 1.12).

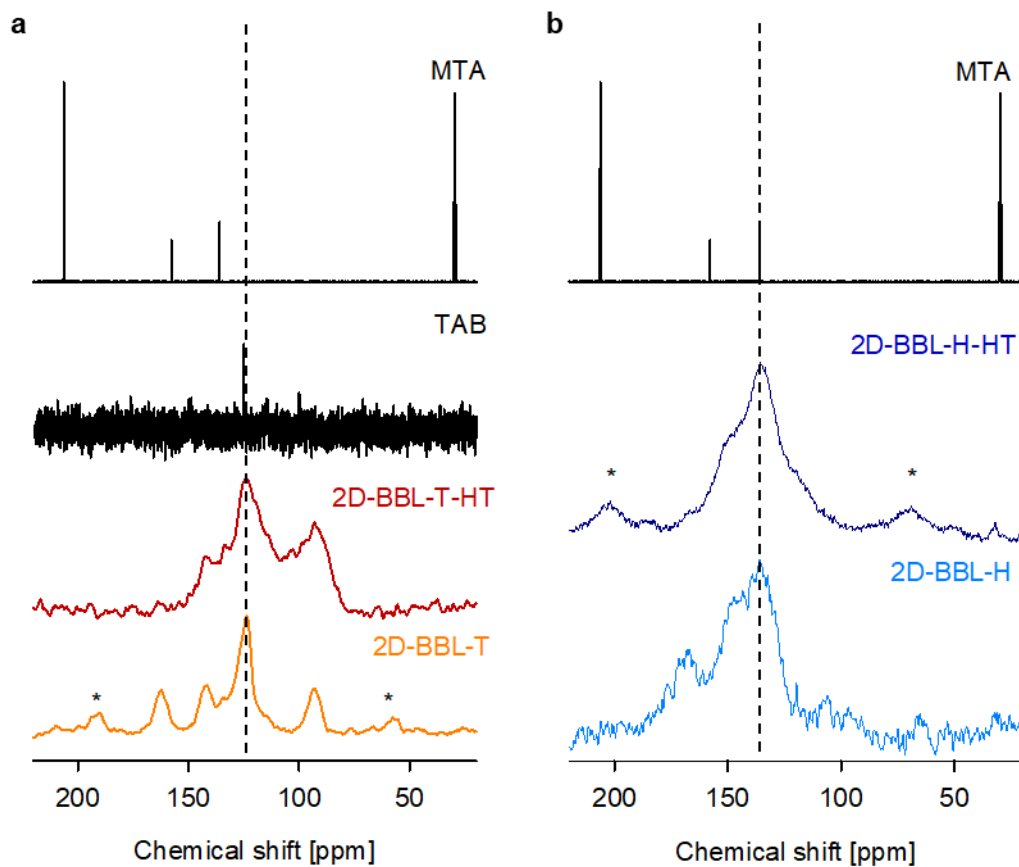


**Figure 1.9.** (a) Solution-state  $^{13}\text{C}$ -NMR spectra of MTA (acetone- $d_6$ ) and TAB ( $\text{D}_2\text{O}$ ) and solid-state  $^{13}\text{C}$ -NMR spectra of 2D-BBL-T and after heat treatment, 2D-BBL-T-HT from the region between 220 and 20 ppm. (b) Solution-state  $^{13}\text{C}$ -NMR spectra of MTA (acetone- $d_6$ ). NMR spectra of HAB can not be measured because of sensitivity. Solid-state  $^{13}\text{C}$ -NMR spectra of 2D-BBL-H and after heat treatment, 2D-BBL-H-HT from the region between 220 and 20 ppm.



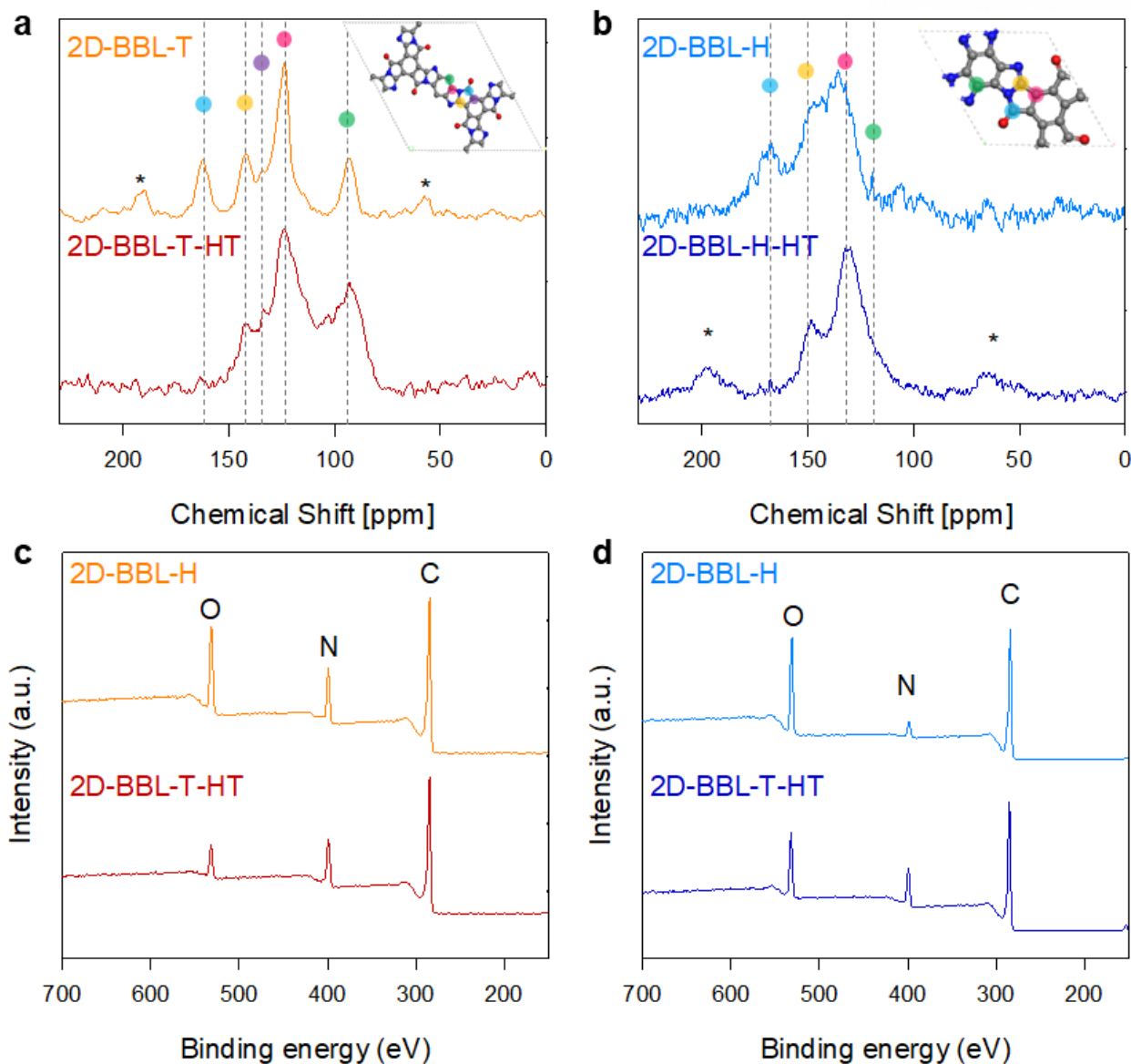


**Figure 1.10.** (a) Solid-state  $^{13}\text{C}$ -NMR spectra of 2D-BBL-T-HT with 2D-BBL-T and (b) 2D-BBL-H-HT with 2D-BBL-H from the region between 220 and 20 ppm. Inset: unit cell structure of BBL polymers and their corresponding carbon atom. Spinning sidebands are indicated by asterisks. XPS full survey (c) 2D-BBL-T-HT with 2D-BBL-T and (d) 2D-BBL-H-HT with 2D-BBL-H.

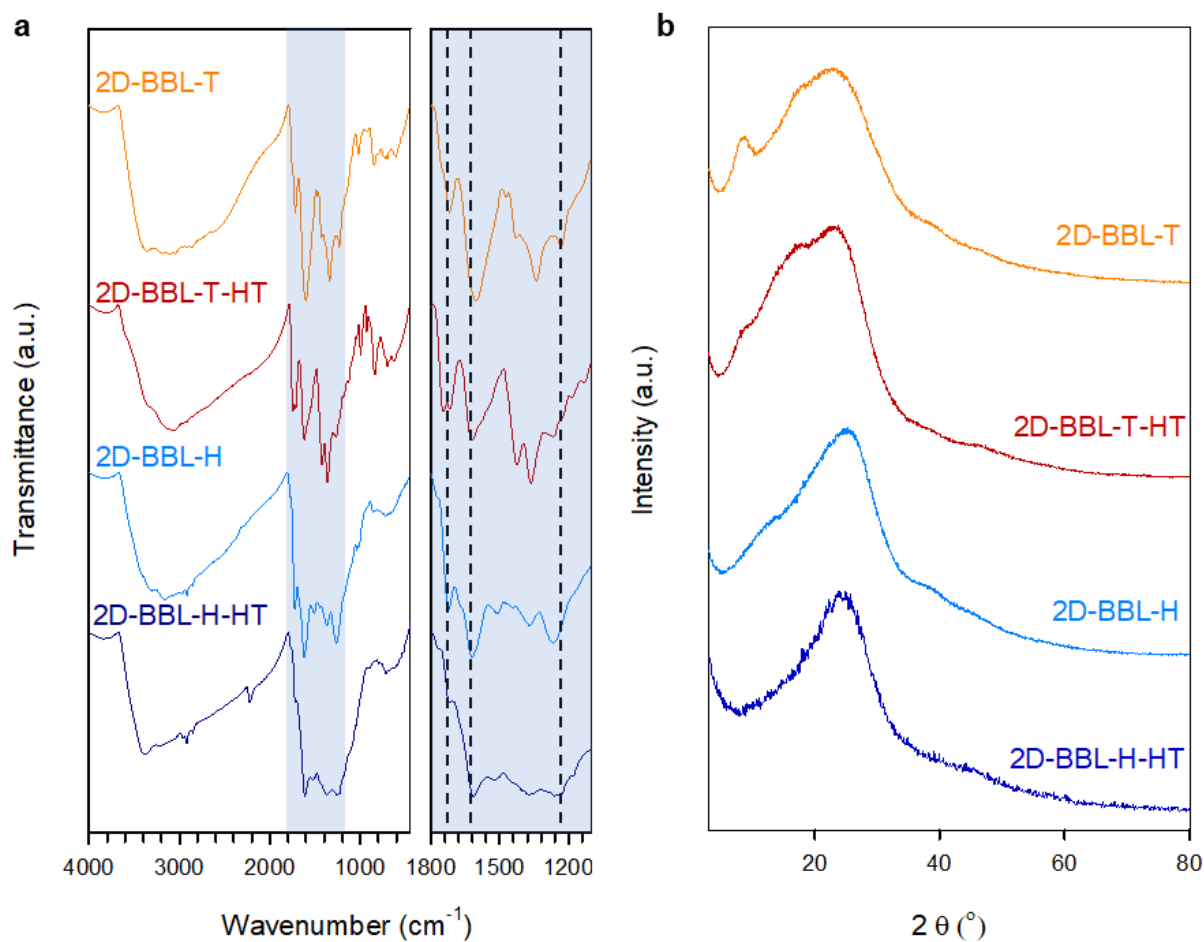


**Figure 1.11.** (a) FT-IR full spectra of 2D-BBL-T, 2D-BBL-T-HT, 2D-BBL-H and 2D-BBL-H-HT; (b) PXRD patterns of 2D-BBL-T, 2D-BBL-H and their annealed samples, 2D-BBL-T-HT and 2D-BBL-H-HT.

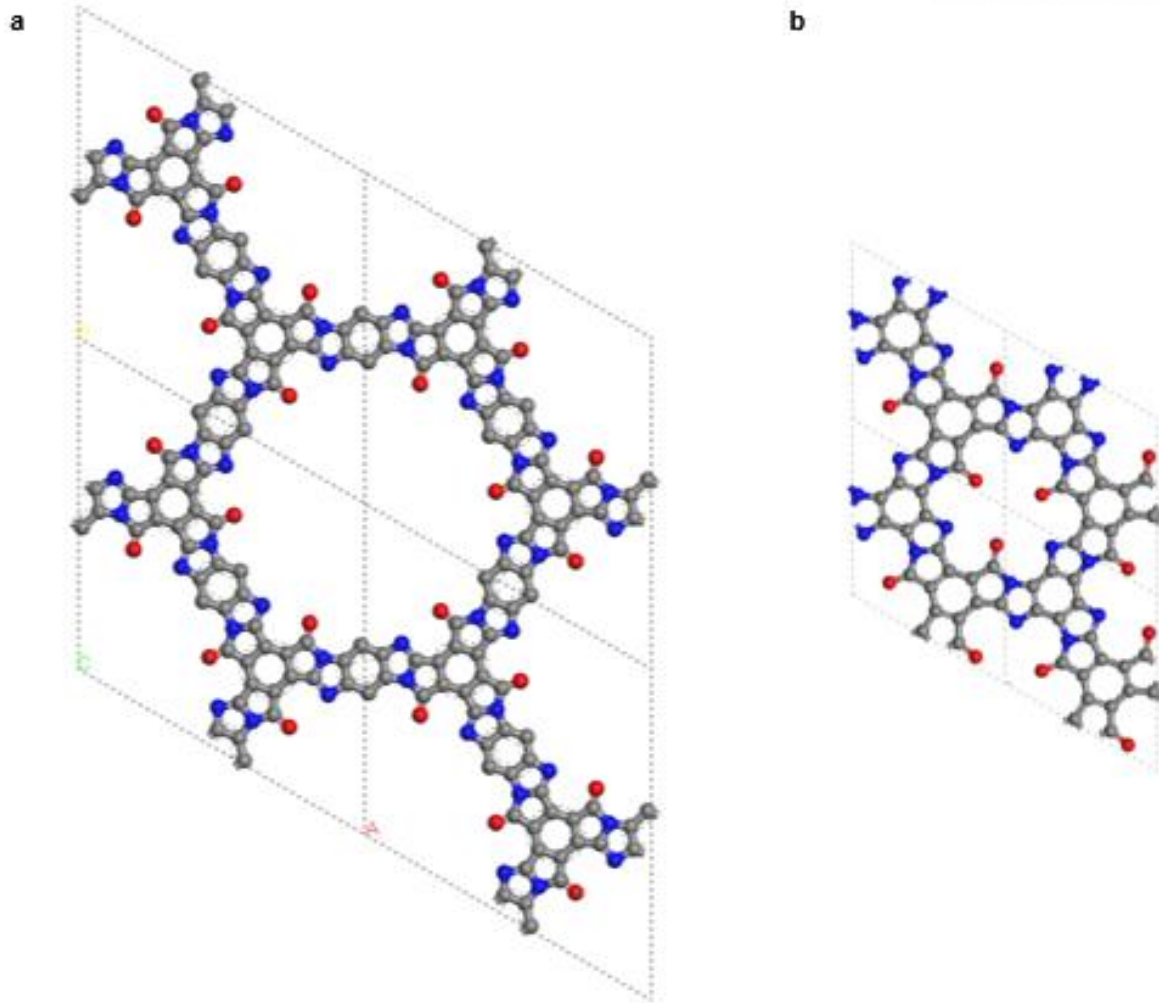


**Figure 1.12.** Simulated unit cell structure of (a) 2D-BBL-T-HT and (b) 2D-BBL-H-HT (C, grey; N, blue; O, red).

For more detailed analysis of bonding nature of both frameworks before (Figure 1.13 and 1.14) and after heat treatment (Figure 1.15 and 1.16) were further examined by XPS. All samples showed distinct three peaks, corresponding to the presence of C 1s, N 1s and O 1s and spectra were calibrated to C 1s peak centered at 284.2 eV. One notable change after the heat treatment is the considerable decreased intensity of the O 1s peak, while the intensity of nitrogen peak relatively increased. These results demonstrated that considerable trapped oxygen contain solvent and edge groups were removed (Figure 1.10c and 1.10d). High-resolution XPS spectra of C 1s further indicated that -COOH peak at 288.1 eV (Figure 1.13b and 1.15b) for 2D-BBL-T-HT and peak at 288.3 eV (Figure 1.14b and 1.16b) for 2D-BBL-H-HT was dramatically decreased. The high-resolution survey spectra of N 1s showed that peak from C=N and C-N peak from imidazole ring remained almost the same before and after heat treatment while the peak intensity from edge amine slightly decreased (Figure 1.13b and 1.15b for 2D-BBL-T-HT and Figure 1.14b and 1.16b for 2D-BBL-H-HT). In the O 1s high-resolution XPS survey, C=O and -CO<sub>2</sub>H peaks were observed for all samples after heat treatment. The peak related to -CO<sub>2</sub>H peak slightly decreased, implying that edge carboxyl groups were selectively removed but some dicarboxylic acid groups dehydrate to form dianhydride with the release of water<sup>35, 39</sup>. (Table 1.2 and 1.3) Despite thermal treatment, oxygen contents did not attain theoretical oxygen containing amount because of their structural hygroscopic nature as we verified from TGA results (Figure 1.6). X-ray diffraction (XRD) patterns showed broad  $2\theta$  [002] peak of 2D-BBL-T-HT and 2D-BBL-H-HT appeared at 23.7° and 25.7° (corresponding to the layer-to-layer distance of 3.75 Å and 3.51 Å) (Figure 1.11b). The experimental *d*-spacings are good in agreement with the linear BBL<sup>40-41</sup>.

The elemental composition of 2D-BBL-T-HT and 2D-BBL-H-HT were calculated from their unit cell structure (Figure 1.12) and analyzed experimentally by elemental analysis (EA), X-ray photoelectron spectroscopy (XPS) and energy dispersive X-ray spectroscopy (EDXS) from SEM (Table 1.2 and 1.3). In all experiments, phosphorus which can originate from PPA was not detected and it proves complete removal of PPA during the rigorous work-up process. Carbon and oxygen contents have differences in both polymer because their hygroscopic natures adsorbed oxygen containing moieties, but their C/N ratio were well matched with theoretical value (C/N = 3). (Table 1.2 and 1.3) After heat treatment, all data showed much good agreement with expected elemental composition and it indicated that 2D-BBL-T and 2D-BBL-H were synthesized as expected holey two-dimensional conjugated structure.

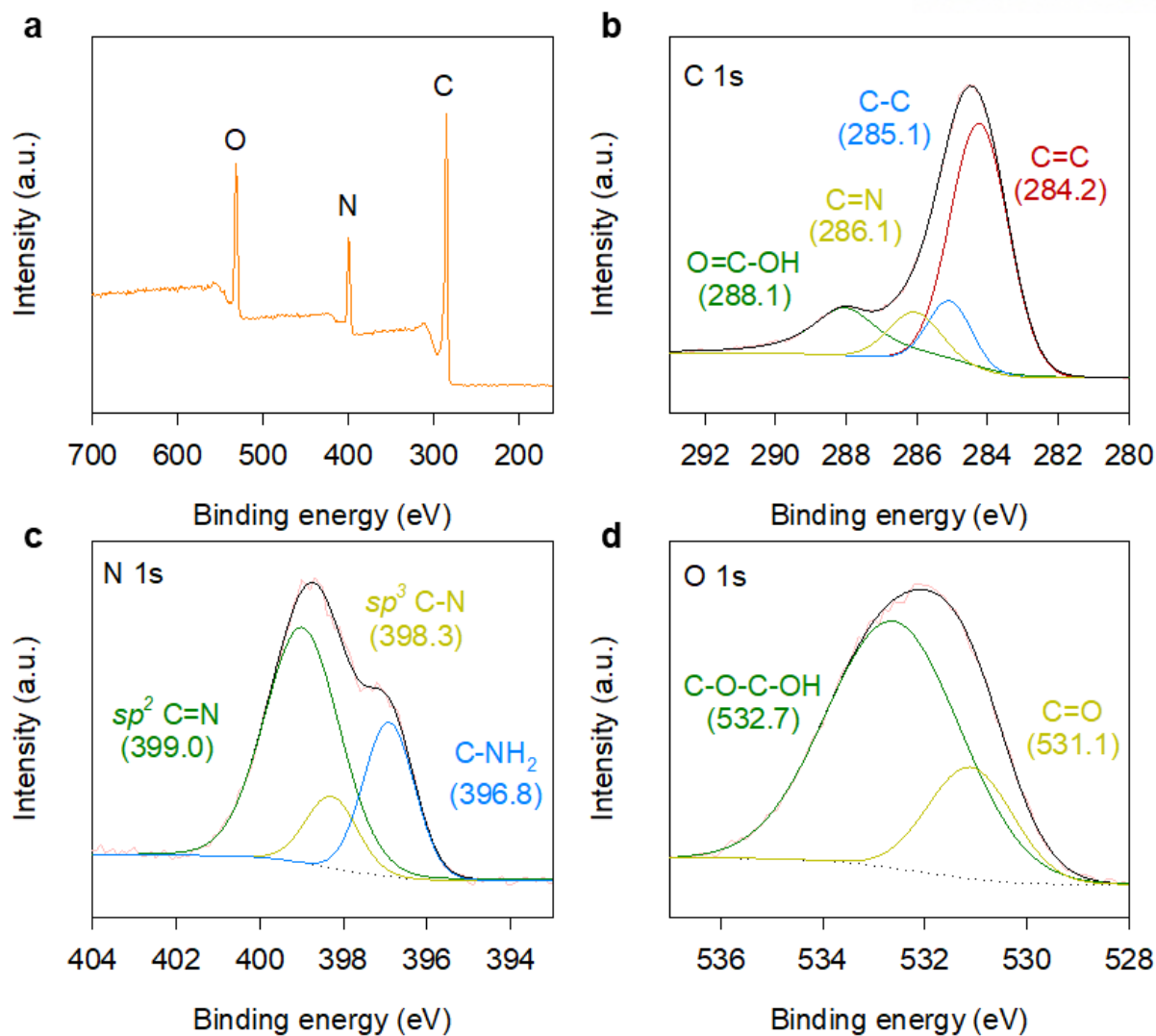


**Figure 1.13.** XPS spectra of 2D-BBL-T: (a) Full survey spectra; High-resolution (b) C 1s, (c) N 1s and (d) O 1s spectra.

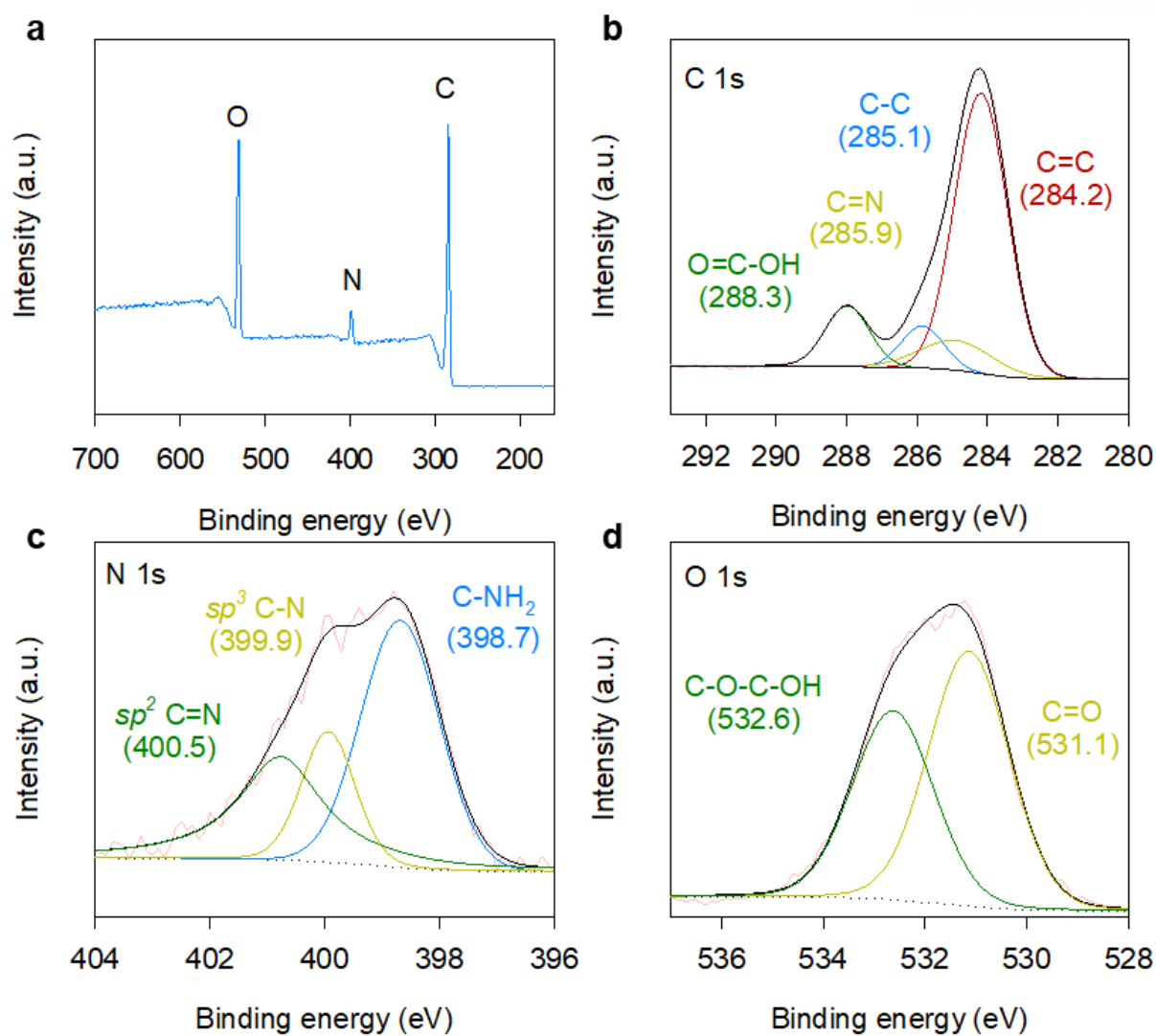


**Figure 1.14.** XPS spectra of 2D-BBL-H: (a) Full survey spectra; High-resolution (b) C 1s, (c) N 1s and (d) O 1s spectra.

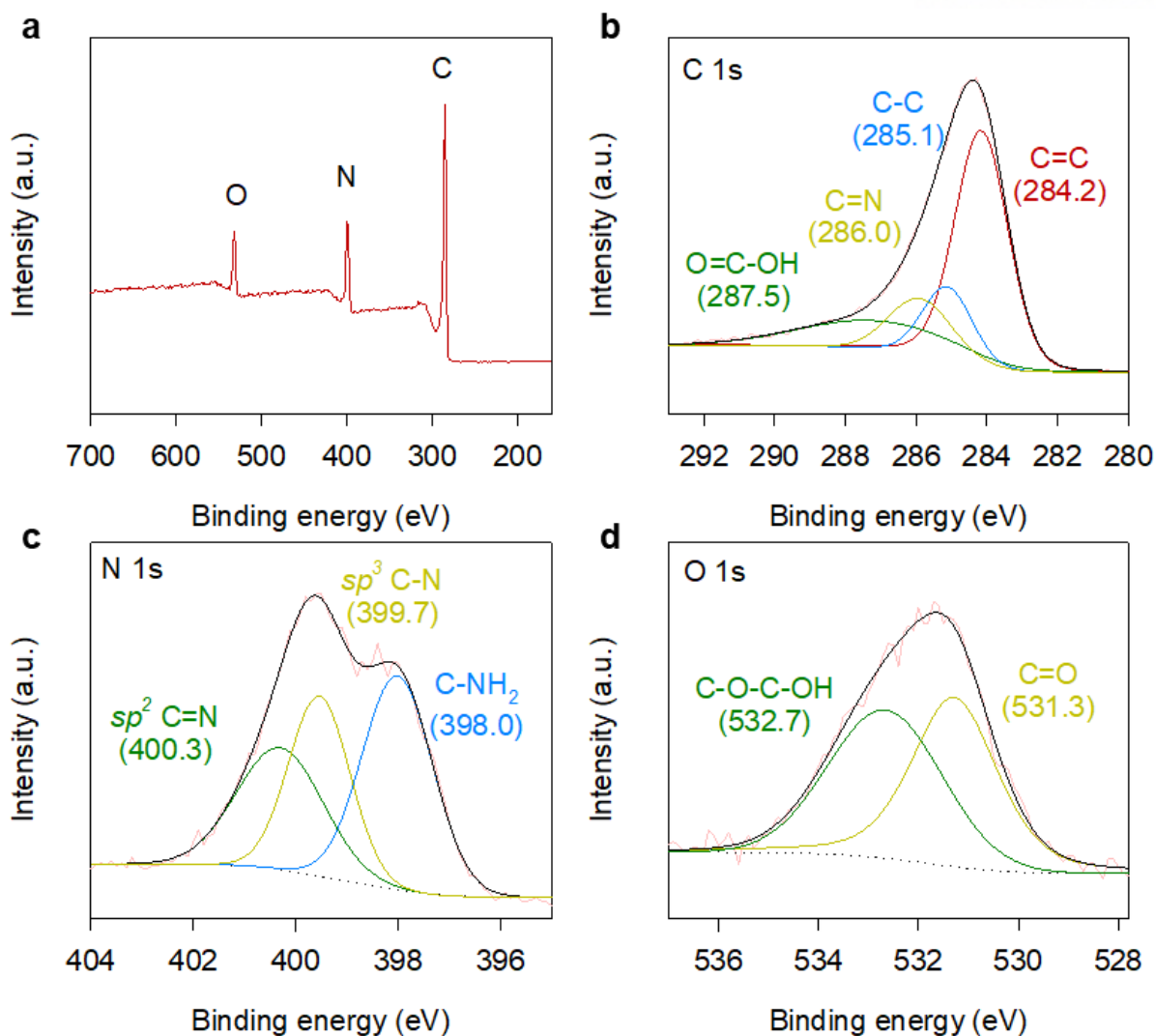


**Figure 1.15.** XPS spectra of 2D-BBL-T-HT: (a) Full survey spectra; High-resolution (b) C 1s, (c) N 1s and (d) O 1s spectra.

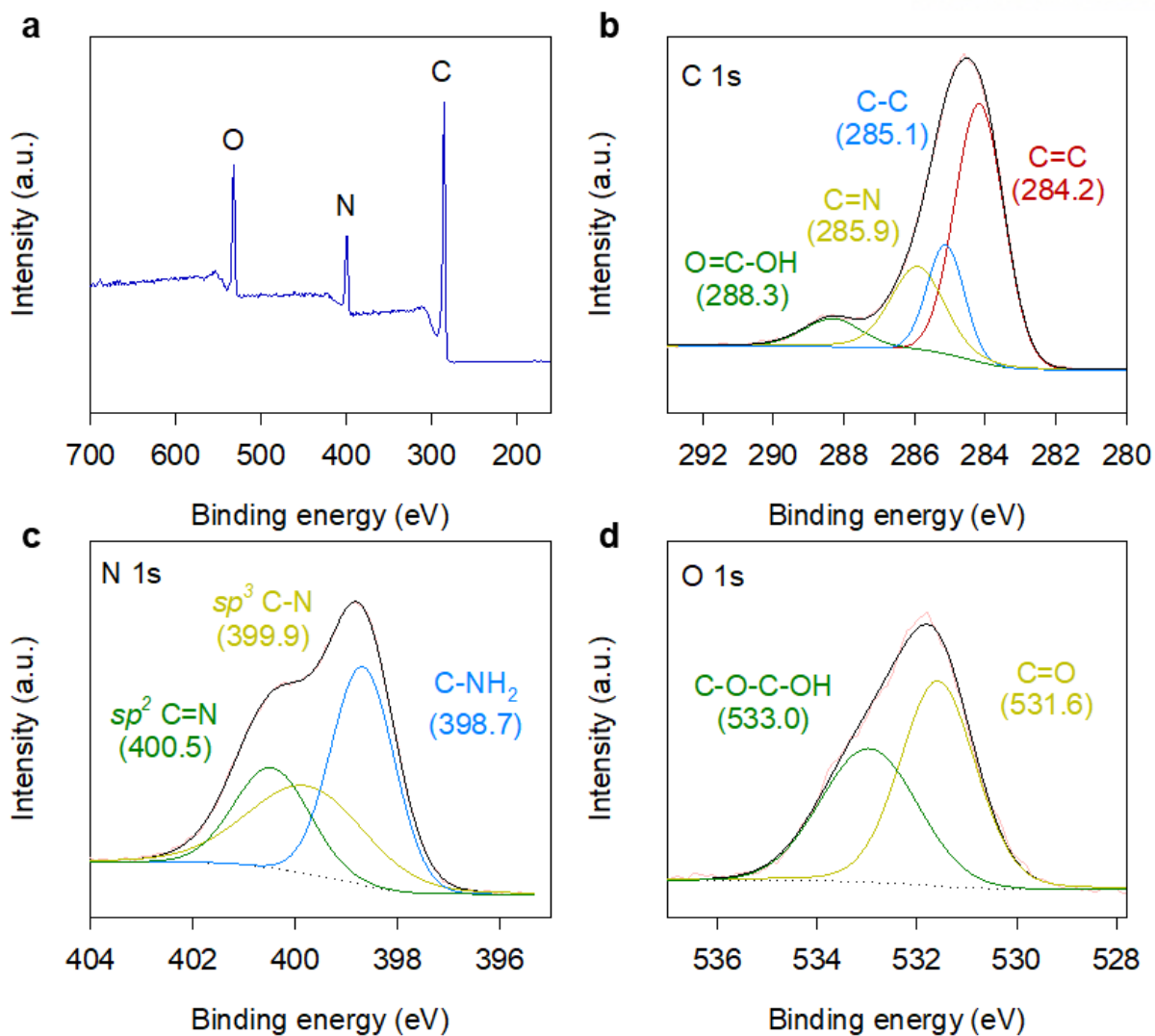


**Figure 1.16.** XPS spectra of 2D-BBL-H-HT: (a) Full survey spectra; High-resolution (b) C 1s, (c) N 1s and (d) O 1s spectra.



**Table 1.2.** Elemental compositions of 2D-BBL-H and 2D-BBL-H-HT.

	<b>Element</b>	<b>C</b>	<b>N</b>	<b>O</b>	<b>H</b>	<b>C/N ratio</b>
<b>2D-BBL-T</b>	Theoretical (wt.%)	65.13	21.70	12.39	0.78	3.00
	XPS (wt. %)	66.18	14.36	19.46	–	4.60
	EA (wt. %)	49.05	16.62	30.52	3.74	2.95
	SEM EDXS (wt.%)	61.93	14.50	23.57	–	4.27
<b>2D-BBL-T-HT</b>	Theoretical (wt.%)	65.13	21.70	12.39	0.78	3.00
	XPS (wt. %)	71.57	18.77	9.66	–	3.81
	EA (wt. %)	60.00	20.75	12.25	3.20	2.89
	SEM EDXS (wt.%)	63.96	15.13	20.91	–	4.23

**Table 1.3.** Elemental compositions of 2D-BBL-H and 2D-BBL-H-HT.

	<b>Element</b>	<b>C</b>	<b>N</b>	<b>O</b>	<b>H</b>	<b>C/N ratio</b>
<b>2D-BBL-H</b>	Theoretical (wt.%)	65.13	21.70	12.39	0.72	3.00
	XPS (wt. %)	66.94	6.52	26.54	–	10.27
	EA (wt. %)	49.47	16.66	27.30	3.25	2.97
	SEM EDXS (wt.%)	54.48	14.02	31.50	–	3.88
<b>2D-BBL-H-HT</b>	Theoretical (wt.%)	65.13	21.70	12.39	0.78	3.00
	XPS (wt. %)	66.69	14.91	18.40	–	4.47
	EA (wt. %)	55.37	23.01	18.48	2.52	2.40
	SEM EDXS (wt.%)	58.61	19.11	22.28	–	3.07

The specific surface area ( $S_{\text{BET}}$ ) and permanent porosity of 2D-BBL-T-HT and 2D-BBL-H-HT was investigated by physical adsorption/desorption isotherm at 77 K by using Brunauer-Emmett-Teller (BET) method. The specific surface area of 2D-BBL-T-HT and 2D-BBL-H-HT were  $611.7 \text{ m}^2 \text{ g}^{-1}$  and  $364.9 \text{ m}^2 \text{ g}^{-1}$ , respectively (Figure 1.17a). Before heat treatment, specific surface area was too small to measure due to the physically absorbed small molecules which are not able to remove by simple pre-annealing at  $150 \text{ }^\circ\text{C}$ . The BET plot indicated that both 2D-BBL-T-HT and 2D-BBL-H-HT typical microporous isotherm (type I) and there was no interlayer adsorption and chemisorption. The pore size distribution was derived using the nonlocal density functional theory (NLDFT) method. The simulated inter hole distance of 2D-BBL-T-HT and 2D-BBL-H-HT was expected 2.1 nm and 1.0 nm respectively (Figure 1.12). As shown in the inset graph in Figure 1.17a, a narrow distribution of micropores was centered at 1.46 nm and 1.09 nm which are comparable with their simulated structure.

Their intrinsic microporosity and polar functional moieties such as  $-\text{NH}_2$ ,  $-\text{OH}$ ,  $-\text{COOH}$ , and nitrogen-rich functionalities in the structure were usually utilized as a gas adsorbent<sup>42-43</sup>. In principles, nitrogen-rich porous organic materials such as triazine, imidazole, imide and azo compounds exhibit high  $\text{CO}_2$  adsorption because cyclic nitrogen interacts strongly with carbon atoms of  $\text{CO}_2$ . In case of hydrogen, the weak interaction between hydrogen and material allow reversibility of adsorption which enables to store and release hydrogen but led to low hydrogen density in ambient conditions. Increasing the interaction between hydrogen and surface of the material is one of the strategy to solve this problem. Ketone and heterocyclic N atom introduced 2D-BBL with intrinsic microporosity can enhance storing hydrogen at atmospheric condition and pore size reducing further improve hydrogen uptake by increasing heat of adsorption<sup>44-46</sup>

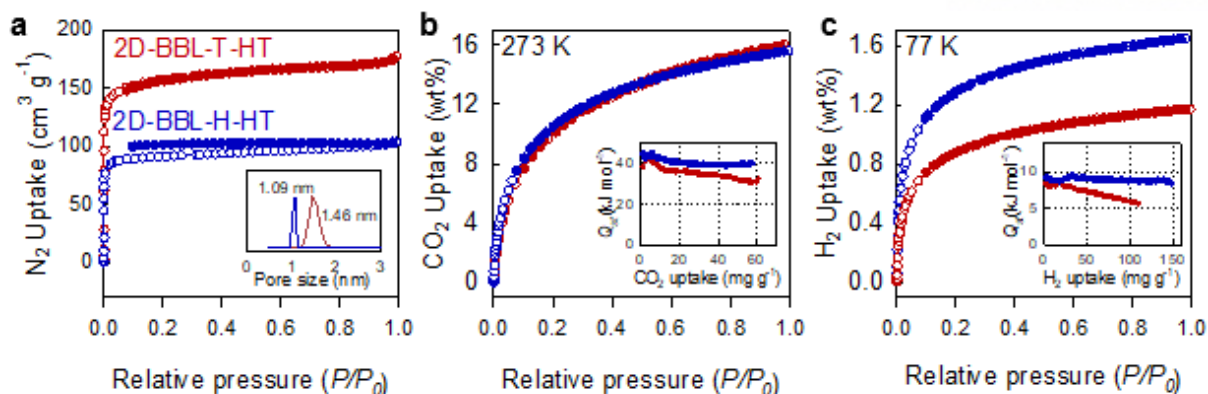


**Figure 1.17.** Permanent porosities of 2D-BBL-T-HT (red) and 2D-BBL-H-HT (blue). (a) Nitrogen adsorption (open circles) and desorption (filled circles) isotherms at 77 K. Inset: pore size distribution calculated from NLDFT. (b) CO<sub>2</sub> adsorption-desorption isotherms at 273 K. Inset:  $Q_{st}$  for CO<sub>2</sub> as a function of gas uptake estimated from low-pressure isotherms at 273 K and 298 K. (c) H<sub>2</sub> adsorption-desorption isotherms at 77 K. Inset:  $Q_{st}$  for H<sub>2</sub> as a function of gas uptake estimated from low-pressure isotherms at 77 K and 87 K.

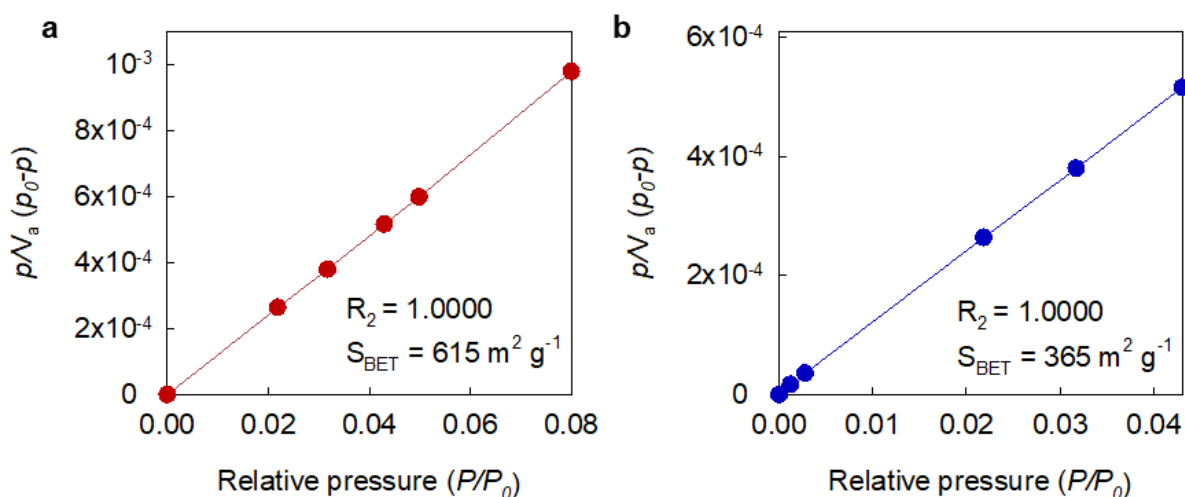


**Figure 1.18.** BET plot of (a) 2D-BBL-T-HT and (b) 2D-BBL-H-HT at 77 K using nitrogen as adsorbate.

The CO<sub>2</sub> and H<sub>2</sub> uptake ability of the 2D-BBL-T-HT and 2D-BBL-H-HT were explored and their isosteric heat of adsorption ( $Q_{st}$ ) for CO<sub>2</sub> and H<sub>2</sub> were calculated from the gas adsorption by using Clausis-Clapeyron equation to understand interactions between 2D-BBL network and gas molecules<sup>47</sup>. The CO<sub>2</sub> adsorption isotherm were found 16.0 wt.% (80.93 cm<sup>3</sup> g<sup>-1</sup>) for 2D-BBL-T-HT and 15.6 wt.% (78.90 cm<sup>3</sup> g<sup>-1</sup>) at 273 K for 2D-BBL-H-HT (Figure 1.17b). The uptake at 298 K showed CO<sub>2</sub> capacity of 8.88 wt.% (44.91 cm<sup>3</sup> g<sup>-1</sup>) for 2D-BBL-T-HT and 10.97 wt.% (55.49 cm<sup>3</sup> g<sup>-1</sup>) for 2D-BBL-H-HT (Figure 1.18b and 1.18d). The  $Q_{st}$  value for CO<sub>2</sub> was estimated from the adsorption data collected at 273 and 298 K near zero relative pressure as 37.80 kJ mol<sup>-1</sup> remained above 32.08 kJ mol<sup>-1</sup> for 2D-BBL-T and 44.43 kJ mol<sup>-1</sup> remained above 39.81 kJ mol<sup>-1</sup> for 2D-BBL-H-HT until full loading up to 1 bar (Figure 1.17b inset). The high  $Q_{st}$  value are indicative of the strong affinity of CO<sub>2</sub> molecules for the 2D BBL frameworks with complete reversibility which implies that functionalization of pores is a considerable factor beyond large surface area<sup>47-48</sup>.

The H<sub>2</sub> adsorption isotherm were found to be 1.18 wt.% (132.0 cm<sup>3</sup> g<sup>-1</sup>) for 2D-BBL-T-HT and 1.65 wt.% (185.4 cm<sup>3</sup> g<sup>-1</sup>) for 2D-BBL-H-HT at 77 K (Figure 1.17c). Even at higher temperature (87 K), adsorption ability of 2D-BBL-H-HT was 1.30 wt.% (145.7 cm<sup>3</sup> g<sup>-1</sup>) which is more than that of 2D-BBL-T-HT (0.97 wt.%; 108.8 cm<sup>3</sup> g<sup>-1</sup>) (Figure 1.18a and 1.18c). The  $Q_{st}$  for H<sub>2</sub> was examined by using the hydrogen adsorption data collected at 77 and 87 K (Figure 1.17c inset). The 2D-BBL-T-HT and 2D-BBL-H-HT displayed a  $Q_{st}$  value of 8.32 kJ mol<sup>-1</sup> and 9.24 kJ mol<sup>-1</sup> at first and decreased as hydrogen uptake increased and recorded the value of 5.67 kJ mol<sup>-1</sup> and 8.49 kJ mol<sup>-1</sup>. Their  $Q_{st}$  values are similar but shows higher affinity toward gas molecule compared with linear BBL structures for all gas<sup>32, 49</sup>. The high  $Q_{st}$  value can be demonstrate the interactions between hydrogen and 2D-BBL networks and adsorption capacity is higher for small pore of 2D-BBL-H-HT (1.0 nm) than 2D-BBL-T-HT (1.5 nm) due to increasing adsorption enthalpies<sup>46</sup>.

Notably in hydrogen uptake experiment, 2D-BBL-H-HT showed much higher adsorption than 2D-BBL-T-HT in the same ambient condition owing to its smaller pore diameter. To the best of our knowledge, it is the first report where the experimental results available to show the decrease of  $Q_{st}$  value with increasing pore diameter in porous materials. The reasons of high uptake are the strong interactions of H<sub>2</sub> with the adsorbent which come from relatively large of binding sites per specific surface area and robust fused-aromatic frameworks with open pores.

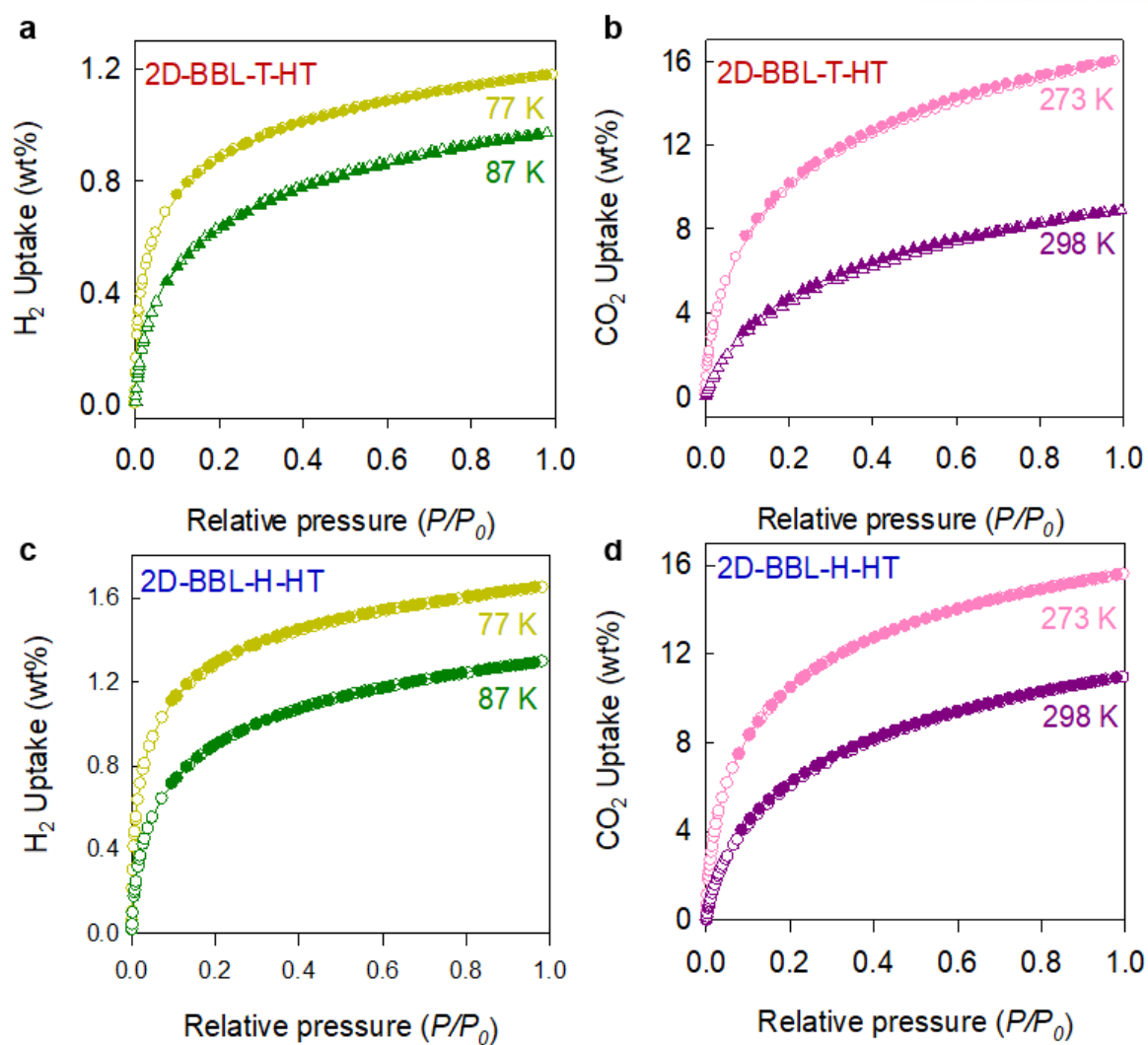


**Figure 1.19.** Permanent porosities of 2D-BBL-T-HT: (a) H<sub>2</sub> adsorption-desorption isotherms at 77 K and 87 K; (b) CO<sub>2</sub> adsorption-desorption isotherms at 273 K and 298 K. Permanent porosities of 2D-BBL-H-HT; (c) H<sub>2</sub> adsorption-desorption isotherms at 77 K and 87 K; (d) CO<sub>2</sub> adsorption-desorption isotherms at 273 K and 298 K.

Given the high porosity and stability of BBLs, we investigated their potential application for the removal of dangerous ion and harmful organic pollutant. As a model ion,  $\text{MnO}_4^-$  was chosen to study inorganic ion capture ability because  $\text{MnO}_4^-$  ion is widely used as disinfectant and deodorizing materials to control taste and odors and remove color for drinking water treatment in forms of potassium permanganate<sup>50</sup>. For selective capturing of organic dye pollutants which can be represented to harmful and toxic water pollutants<sup>51</sup>, methylene blue (MB) and methyl orange (MO) with the dimensions of  $13.9 \times 14.4 \times 24.5 \text{ \AA}$  and  $5.4 \times 7.8 \times 15.2 \text{ \AA}$ , respectively<sup>52</sup>. On the basis of a size exclusive effect, 2D-BBL-T-HT and 2D-BBL-H-HT were examined and evaluated their capture ability in size-selective ion capture. Here, the ionic removal was performed with 3 mL of aqueous solution of  $\text{KMnO}_4$  (0.25 mM) with 2D-BBL-T and 2D-BBL-H at room temperature for 5 min by using UV-vis spectrometer. As shown in Figure 1.20a,  $\text{MnO}_4^-$  was hardly removed by 2D-BBL-H-HT however, 2D-BBL-T-HT can be removed  $\sim 73\%$  of  $\text{KMnO}_4$ . Beyond the fast anion uptake, 2D-BBLs were subjected to selectively capture MB and MO. The experiment was performed with 3 mL of aqueous solution of MB and MO (0.01 mM) and selectivity was examined by using mixture of 3 mL two dyes (1 mL of MB and MO was taken with the same molar concentration.) at room temperature for 5 min. (Figure 1.20b and 1.20c) UV-vis spectra showed that, only 2D-BBL-T almost completely capture the MB molecules ( $\sim 1.3\%$ ) in about 5 min, whereas MB molecules filtered out into the solution, which is indicated that size discrimination ability of 2D-BBL-T-HT. UV-vis spectra after dye adsorption measurement shows over 100% which originated from small particles of 2D-BBLs penetrated after filtration. In addition, MB/MO mixture solution were successfully separated by simply passing through 2D-BBL-T-HT equipped syringe filter. (Figure 1.20d and 1.20g)

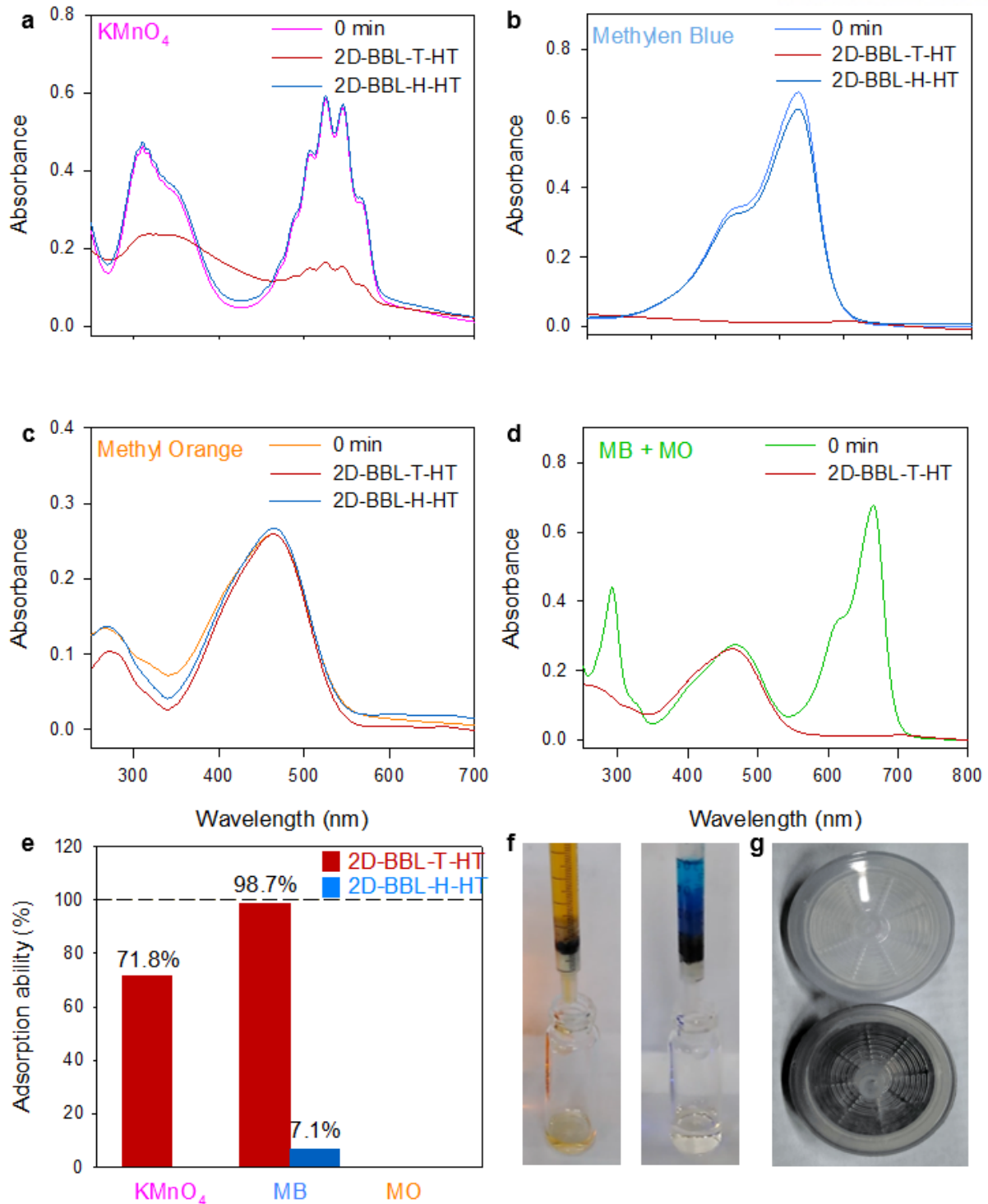


**Figure 1.20.** UV-vis spectra of (a)  $\text{MnO}_4^-$ , (b) Methylene blue and (c) Methyl orange aqueous solution in the presence of 2D-BBL-T-HT (red line) and 2D-BBL-H-HT (blue line) for 5 min. (d) UV-vis spectra of MB/MO aqueous solution in the presence of 2D-BBL-T-HT for 5 min. (e) Comparison of the dye adsorption ability of 2D-BBL-T-HT (red) and 2D-BBL-H-HT (Blue). Digital photographs of (f) dye adsorption test by using 2D-BBL-T-HT and (g) 5mg of 2D-BBL-T-HT equipped filter.

## | Conclusion

Two-dimensional poly(benzoimidazo benzophenanthroline) (2D-BBL) were designed as dimension expanded BBL polymer and successfully synthesized *via* double condensation reaction between amine (-NH<sub>2</sub>) and mellitic trianhydride (MTA) in polyphosphoric acid (PPA) medium. For activation, edge functional groups were selectively removed by heat treatment and obtained sheet-like shape organic network structure. The extended 2D BBL structures have permanent porosity with a BET surface area of over 615 m<sup>2</sup> g<sup>-1</sup> for 2D-BBL-T-HT and over 365 m<sup>2</sup> g<sup>-1</sup> for 2D-BBL-H-HT and the pore size matches well with the expected structure. Though the chemical nature of the 2D BBLs is similar but owing to heteroatom-rich pore texture per specific surface area and microporous aromatic heterocyclic structure, 2D-BBL-H-HT possess high affinity towards hydrogen and displays high adsorption capacity for H<sub>2</sub> (1.65 wt.%, at 77 K and 1 bar) and CO<sub>2</sub> (15.6 wt.%, at 273 K and 1 bar). Based on their size exclusive effect, 2D-BBL-T-HT showed almost complete capturing ability of methylene blue (MB) over methyl orange (MO). In summary, the strategy to extend conjugated ladder polymer into two-dimension by using the effective condensation reaction have the possibility to utilize rigid ladder polymer with tailored properties for future applications.



## Chapter 2 Synthesis of triphenylene-based covalent triazine networks (sTP-CTN) in the presence of gaseous HCl *via* solid state cyclotrimerization.

### | Abstract

Solid-state reaction of triphenylene-2,3,6,7,10,11-hexacarbonitrile (THCN) is carried out in a sealed glass ampoule in the presence of gaseous hydrochloric acid (HCl) to synthesize conjugated triazine-based networks (CTN-0). THCN is successfully synthesized and recrystallized to make single crystal, and their structure is solved by using single crystal XRD. The CTN-0 is compared with Zn-CTN prepared by conventional synthetic methodology in the presence of ZnCl<sub>2</sub> and analyzed by using various analysis.

### | Introduction

Triphenylene are well known compound for discotic liquid crystal filed and they show typical columnar mesophase in most cases because of strong  $\pi$ - $\pi$  interactions for the flat, rigid aromatic core structures<sup>53-54</sup>. Triphenylene-based covalent organic networks (CONs) was synthesized by using monomers which are hexa-substituted with bromine, alkoxide, hydroxide, etc<sup>55</sup>. The cyclization is enthalpically favored by the aromatic character of the central ring and the greater conjugation of the planar triphenylene relative to nonplanar acyclic oligomers and polymers. Since the advent of new heteroatom-doped carbon materials, various attempts to synthesis and control their properties issue a challenge to develop potential applications.

Recently, synthesis of structural well-defined covalent triazine networks discovered in 2008<sup>56</sup> and attracts many interests to be used as tailored-functional materials because they possess high porosity, good thermal and chemical stability, high nitrogen contents for doping effects and expected versatile applications such as CO<sub>2</sub> capture, energy storage materials<sup>57</sup> and catalysis<sup>58</sup>. In short, there are synthetic strategies for synthesis triazine based material from aromatic nitriles, for instance, the ionothermal reaction with zinc chloride (ZnCl<sub>2</sub>)<sup>59</sup> and solvothermal cyclotrimerization. Ionothermal reaction condition requires stoichiometric amounts of zinc chloride that are difficult to remove. While, solvothermal reactions are carried out in highly corrosive environment such as trifluoromethane sulfonic acid (CF<sub>3</sub>SO<sub>3</sub>H)<sup>60-61</sup>.

New synthetic approaches appear to overcome these issues, for example, element-sulfur mediated synthesis<sup>62</sup>, P<sub>2</sub>O<sub>5</sub> catalyzed reaction<sup>63</sup> and direct arylation coupling approach<sup>58, 64</sup>. Here, triphenylene-2,3,6,7,10,11-hexacarbonitrile (THCN) was prepared as a building block which has hexa- nitrile functional groups to synthesize of triphenylene-based conjugated triazine networks (sTP-CTN). By using dry gaseous hydrochloric acid (HCl) as a catalyst, CTN-0 successfully synthesized and formed s-

triazine in the network. In this approach, compared with the triazine networks (Zn-CTN) which synthesized in molten Lewis acid,  $\text{ZnCl}_2$ . The CTN-0 prepared in this work provide a new strategy to synthesize triazine-based networks with many advantages over typical methods.

## | Experimental Section

### 2.3.1 Materials

All solvents and reagent for synthesis were commercially available and used without further purification, unless otherwise specified. Triphenylene was purchased from Alfa Aesar (Product #: L00955, 98% purity) and used as received. Bromine ( $\text{Br}_2$ ) was purchased from SUNSEI Chemical Inc. (Product #: 37175-0301, 99.0%+ purity) and used as received.

### 2.3.2 Instrument

$^1\text{H}$ -NMR and  $^{13}\text{C}$ -NMR were obtained on a 400 MHz FT-NMR AVANCE III HD (Bruker, USA) spectrometer. Solid Carbon NMR were recorded on a 600 MHz FT-NMR VNMRS 600 (Varian, USA) spectrometer. Thermogravimetric analysis (TGA) was conducted on a PerkinElmer STA 8000 with a ramping rate of  $10\text{ }^\circ\text{C min}^{-1}$  under air or nitrogen. Elemental analysis (EA) was conducted with Flash 2000 (Thermo Scientific, Netherlands). The field emission scanning electron microscope (FE-SEM) was obtained by using a Nanonova 230 (FEI, USA). X-ray photoelectron spectroscopy (XPS) was performed on an X-ray photoelectron spectrometer (K-alpha, Thermo Fisher Scientific, UK). X-ray diffraction (XRD) patterns were taken on a high-power X-ray diffractometer (D/MAZX 2500 V/PC, Rigaku, Japan) using  $\text{Cu K}\alpha$  radiation (40 kV, 20 mA,  $\lambda = 1.5418\text{ \AA}$ ). Fourier transform infrared (FT-IR) spectra were performed on Spectrum 100 (Perkin-Elmer, USA) with KBr disks pellet.

### 2.3.3 Preparation of 2,3,6,7,10,11-hexabromotriphenylene (TPBr)

In round-bottom flask, triphenylene (2.26 g, 9.91 mmol) and iron powder (0.19 g, 3.60 mmol) in nitrobenzene (80 mL) was stirred under nitrogen atmosphere at room temperature for 10 min. Bromine (4.4 ml, 85.01 mmol) was slowly added into the solution and heated at  $200\text{ }^\circ\text{C}$  for 2 h. Upon cooling to room temperature, reaction mixture was poured into diethyl ether and precipitated, the insoluble white solid was washed with additional diethyl ether and collected by filtration and recrystallized with 1,3,5-trichlorobenzene. Given white powder was obtained 6.20 g, 89.95% of yield<sup>65</sup>.

### 2.3.4 Preparation of triphenylene-2,3,6,7,10,11-hexacarbonitrile (THCN)

To a solution of 2,3,6,7,10,11-hexabromotriphenylene (2.49 g, 3.57 mmol) and Cu(I)CN (7.68 g, 85.75 mmol) in *N,N*-Dimethylformamide (85 mL) was prepared in 3-neck flask equipped with reflux condenser under nitrogen atmosphere and heated to reflux temperature for 30 h. Any insoluble impurity was removed by passing through celite with acetonitrile and evaporated. Collected solid was stirred in small portion of aqueous ethylenediamine solution and filtered, washed with D.I. water and giving pale yellow powder 0.54 g, with the yield of 40%. The solid product was recrystallized by acetonitrile and given yellow needle-type crystal.  $^1\text{H-NMR}$  (Acetone- $d_6$ , 400MHz)  $\delta$  = 9.846 ppm  $^{13}\text{C-NMR}$  (Acetone- $d_6$ , 400MHz)  $\delta$  = 133.06, 132.84, 116.52, 116.32 ppm; FT-IR (KBr pellet) 1500, 1562 (C–C in aromatic), 2236 (C $\equiv$ N), 3060 (C–H in aromatic)  $\text{cm}^{-1}$ . DIP-MS ( $m/z$ , relative intensity) 378 (100) [ $\text{M}^+$ ]. Anal. Calcd. (%) for  $\text{C}_{24}\text{H}_6\text{N}_6$ : C, 76.19; H, 1.60; N, 22.21. Found: C, 76.34; H, 1.50; N, 22.57.

### 2.3.5 Crystallographic data collection and refinement of the structure

A crystal of THCN was coated with paratone oil and the diffraction data measured at 173 K with Mo  $\text{K}\alpha$  radiation on an X-ray diffraction camera system using an imaging plate equipped with a graphite crystal incident beam monochromator. The RapidAuto software<sup>66</sup> was used for data collection and data processing. Structure was solved by direct method and refined by full-matrix least-squares calculation with the SHELX software package<sup>67</sup>.

One triphenylene-2,3,6,7,10,11-hexacarbonitrile and one lattice acetonitrile molecule are observed as an asymmetric unit. All non-hydrogen atoms are refined anisotropically; the hydrogen atoms were assigned isotropic displacement coefficients  $U(\text{H}) = 1.2U(\text{C})$  and  $1.5U(\text{C}_{\text{methyl}})$ , their coordinates were allowed to ride on their respective atoms. Refinement of the structure converged at a final  $R1 = 0.0695$  and  $wR2 = 0.0920$  for 2212 reflections with  $I > 2\sigma(I)$ ;  $R1 = 0.1162$  and  $wR2 = 0.1683$  for all 4539 reflections. The largest difference peak and hole were 0.171 and  $-0.161 \text{ e} \cdot \text{\AA}^{-3}$ , respectively.

A summary of the crystal and some crystallography data is given in Table 2.1. CCDC-\*\*\*\*\* contains the supplementary crystallographic data for this paper. The data can be obtained free of charge at [www.ccdc.cam.ac.uk/conts/retrieving.html](http://www.ccdc.cam.ac.uk/conts/retrieving.html) or from the Cambridge Crystallographic Data Centre, 12, Union Road, Cambridge CB2 1EZ, UK.

### 2.3.6 Synthesis of triphenylene-based conjugated triazine networks (CTN-0) via solid-state polymerization by using dry HCl gas as catalyst.

Triphenylene-2,3,6,7,10,11-hexacarbonitrile (THCN) crystal (200 mg) was placed in a glass

ampoule ( $\Phi 4 \times 14$  cm). The ampoule was repeatedly charged and discharged with argon gas few times and dry hydrogen chloride (HCl) gas generated by following literature<sup>68</sup> was fully charged. The ampoule was flame sealed and placed box furnace. The furnace was gradually heated to 300 °C with heating rate 1.2 °C min<sup>-1</sup> and maintained for 4 h, then further heated to 400 °C for 72 h. After slow cooling, the ampoule was opened for few hours to degasses HCl gas and sample. The shiny black crystal was purified by soxhlet extraction with acetonitrile to remove unreacted monomer and collected by vacuum filtration. The final product obtained was 31 mg (21.06%). Anal. Calcd. (%) for C<sub>24</sub>H<sub>6</sub>N<sub>6</sub>: C, 74.46; H, 2.16; N, 23.38. Found: C, 73.62; H, 1.76; O, 10.31; N, 16.32.

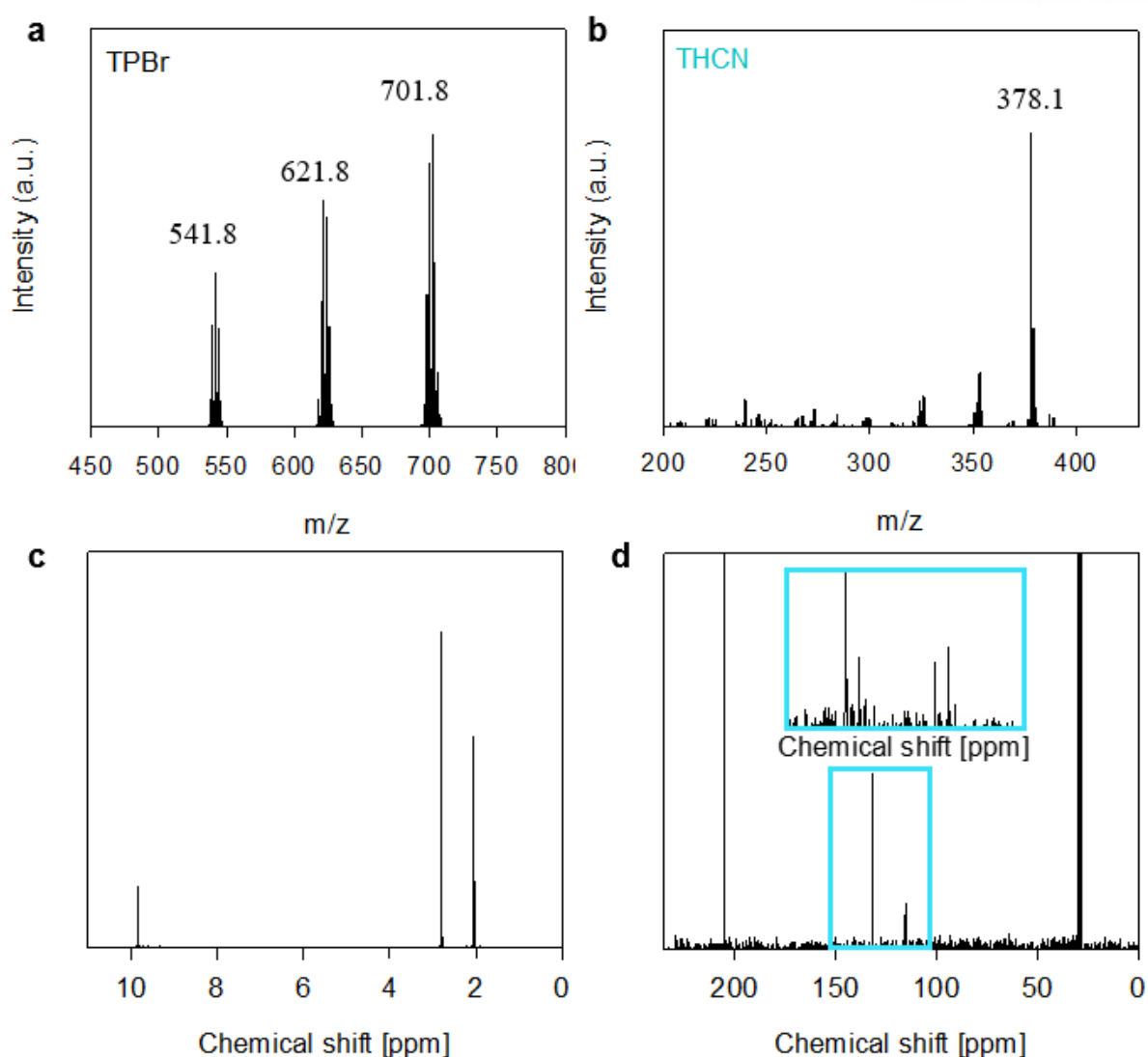
### 2.3.7 Synthesis of triphenylene-based conjugated triazine networks with Zinc chloride (Zn-CTN)

Triphenylene-2,3,6,7,10,11-hexacarbonitrile (THCN) crystal (100 mg) was placed in a glass ampoule ( $\Phi 4 \times 14$  cm) with finely grinded ZnCl<sub>2</sub> (350 mg). The ampoule was repeatedly charged and discharged with argon gas few times to remove air. The ampoule was flame sealed and placed box furnace. The furnace was gradually heated to 300 °C with heating rate 1.2 °C min<sup>-1</sup> and maintained for 4 h, then further heated to 400 °C for 72 h. After slow cooling, the ampoule was opened. The resultant was collected and purified by using 3 M of HCl solution to remove ZnCl<sub>2</sub>. Soxhlet extraction with H<sub>2</sub>O and acetonitrile was used to further purification. The shiny black crystal was obtained.

## | Results and Discussion

Replacing halogen atom to nitrile group by using copper (I) cyanide in high boiling point solvent known as Rosenmund-von Braun reaction is general reaction route<sup>69-71</sup>. Triphenylene-2,3,6,7,10,11-hexacarbonitrile (THCN) was firstly reported in 2000 by Hanack group and known to be given partial exchange mono- to penta-cyano groups in normal Rosenmund-von Braun reaction conditions<sup>72</sup>. Luckily, THCN was successfully synthesized from 2,3,6,7,10,11-hecabromotriphenylene (TPBr) with copper (I) cyanide as a catalyst in *N,N*-Dimethylformamide (DMF) solution. Resulting solid was recrystallized in acetonitrile given highly pure and transparent yellow needle-type crystals. Formation of THCN crystals was confirmed by <sup>1</sup>H and <sup>13</sup>C NMR, MS, IR and elemental analysis. (Figure 2.1 and Table 2.1) In optical microscopy images, THCN crystals shows clear surface and crystal dimension length are longer than 1 mm and some are even longer than 5 mm from the optical microscope image. (Figure 2.5a and 2.5b) The absolute crystal structure of THCN has been solved for the first time by single-crystal X-ray diffraction analysis. (Figure 2.2 and Table 2.1) According to crystallographic information, three adjacent THCN molecules interact and nearest three nitrile groups which having average distance of 4.0 Å (3.4 Å; 4.5 Å; 5.5 Å). (Figure 2.2). Also, grown needle-type crystals contains acetonitrile molecule

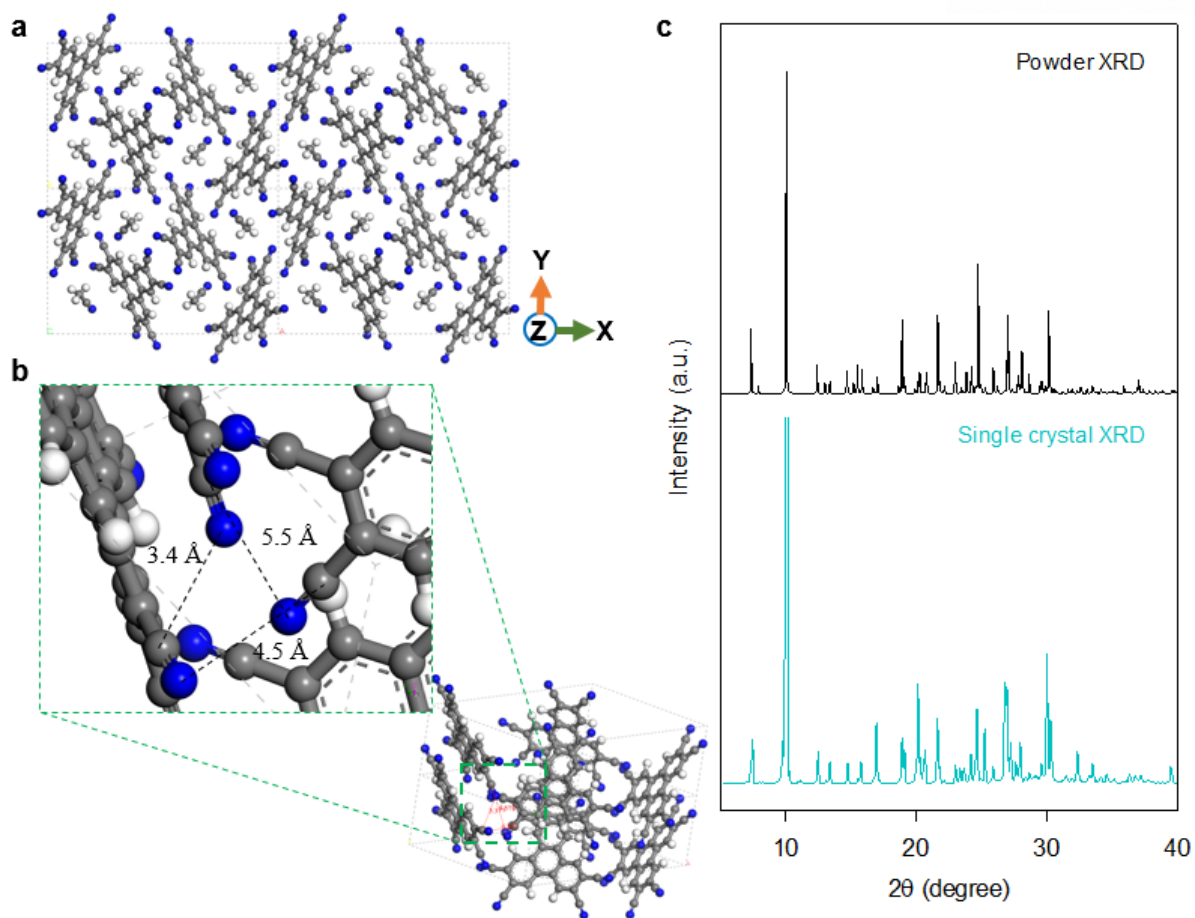
as 1:1 ratio which was used as recrystallization solvent. Thermogravimetric analysis (TGA) showed that 10% of weight loss occur as increased temperature around 100 °C, acetonitrile molecule was evaporated and form empty space inside of the crystal. (Figure 2.3) Cyclotrimerization of nitrile compound typically known to occur above 300 °C but THCN crystal is thermally stable even at 465 °C and started to decompose, not to melt.



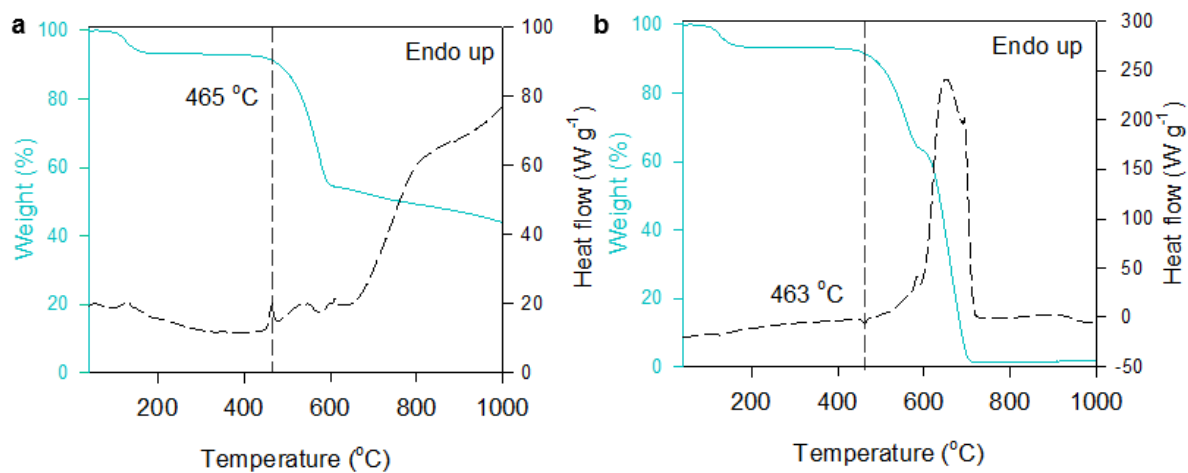
**Figure 2.1.** (a) Electron ionized mass spectroscopy of TPBr, which is 701.8 m/z ( $M^+$ , Calcd. 701.5) and debromination occur during measurement which show at 621.8 and 541.8 m/z peaks by strong electron source. (b) Electron ionized mass spectroscopy of TPCN, which is 378.1 m/z ( $M^+$ , Calcd. 378.1). (c)  $^1\text{H}$ -NMR and (d)  $^{13}\text{C}$ -NMR spectra of triphenylene-2,3,6,7,10,11-hexacarbonitrile (acetone- $d_6$ ).

Table 2.1. Crystallographic data for THCN

Identification	THCN
Empirical formula	C <sub>26</sub> H <sub>9</sub> N <sub>7</sub>
Formula weight	419.40
Temperature	173(2) K
Wavelength	0.71073 Å
Crystal system	Orthorhombic
Space group	<i>Pna</i> 2 <sub>1</sub>
Unit cell dimensions	a = 22.367(5) Å, α = 90° b = 14.264(3) Å, β = 90° c = 6.6547(13) Å, γ = 90°
Volume	2123.1(7) Å <sup>3</sup>
Z	4
Density (calculated)	1.312 Mg m <sup>-3</sup>
Absorption coefficient	0.083 mm <sup>-1</sup>
F(000)	856
Crystal size	0.480 x 0.040 x 0.030 mm <sup>3</sup>
Theta range for data collection	2.998 to 27.471°
Index ranges	-28 ≤ h ≤ 28, -18 ≤ k ≤ 18, -8 ≤ l ≤ 8
Reflections collected	19809
Independent reflections	4539 [R(int) = 0.1568]
Completeness to theta = 25.242°	99.8 %
Absorption correction	Semi-empirical from equivalents
Max. and min. transmission	0.998 and 0.961
Refinement method	Full-matrix least-squares on F <sup>2</sup>
Data / restraints / parameters	4539 / 1 / 300
Goodness-of-fit on F <sup>2</sup>	0.974
Final R indices [I > 2σ(I)]	R1 = 0.0695, wR2 = 0.0920
R indices (all data)	R1 = 0.1683, wR2 = 0.1162
Extinction coefficient	0.0061(13)
Largest diff. peak and hole	0.171 and -0.161 e·Å <sup>-3</sup>



**Figure 2.2.** (a) Ball and stick packing diagram of THCN crystal viewed along the crystallographic z-axis. (b) Diagram of THCN red lines indicate interdigitation between three nitrile functional groups which reaction occur. (color code: grey=carbon; blue=nitrogen; white=hydrogen). (c) Powdered and single crystal X-ray diffraction (XRD) pattern of THCN.



**Figure 2.3.** TGA thermograms of THCN crystals with ramping rate of  $10\text{ }^{\circ}\text{C min}^{-1}$ : (a) in nitrogen and (b) in air.



For cyclotrimerization reaction of nitriles, extreme conditions of high pressure and temperature was required to trimerize aromatic nitrile to form *s*-triazine ring without catalytic reaction<sup>73</sup>. However, with the presence of acid catalysts such as *p*-toluenesulfonic acid<sup>74</sup> trifluoromethylsulfonic acid<sup>60, 75</sup>, phosphorous pentoxide<sup>63</sup>, molten Lewis acid<sup>56</sup>, alkali metals and alkaline earth metal, trimerization of aromatic nitriles can be carried out at moderate temperature and pressure. Recently, there was an attempt to use gaseous hydrogen chloride (HCl) as a trimerization of 1,3,5-tricyanobenzene single crystal in solid-state and successfully synthesized highly stable triazine-based organic superstructures<sup>68</sup>. Inspired benefits of gaseous HCl catalysts for cyclotrimerization of aromatic nitrile compound over other strong acid condition or inefficient work-up process, triphenylene-2,3,6,7,10,11-hexacarbonitrile (THCN) was subjected to synthesize conjugated triazine network *via* solid-state polymerization (sTP-CTN). Acid-catalyzed polymerization of nitriles recently revealed that two-step reaction which firstly form imidoyl chloride functionalized intermediate, RC(NR')Cl, and then, cyclotrimerization into *s*-triazine in solid state<sup>68, 76</sup>.

Using synthetic procedure described in figure 2.4a., triphenylene-2,3,6,7,10,11-hexacarbonitrile (THCN) crystals was placed in the glass ampoule with dry hydrogen chloride (HCl) and step-wisely annealed at 400 °C in closed system. THCN crystals are shiny yellow crystals with clear surface as shown in optical microscopy images (Figure 2.4b, 2.5a and 2.5b) but after reaction, the color of the sample changed to dark black with the high yield of 21.06%. (Figure 2.4d-e and 2.5c-d) Formation of *s*-triazine by trimerization of THCN molecule was confirmed by <sup>13</sup>C magic-angle spinning (MAS) NMR measurements. CTN-0 shows five distinct signals at 167, 132, 121, 115 and 114 ppm which are matched with their proposed structure. (Figure 2.4f) Newly formed *s*-triazine moiety carbon peak at 167 ppm were observed which provide the evidence for successive synthesis of CTN-0. Also, two neighboring carbon in the triphenylene-core induced peak broadening which located at 132 ppm.

On the other hand, THCN crystals were react in the presence of molten Lewis acid, ZnCl<sub>2</sub>, as a reference material for formation of *s*-triazine based network structure named Zn-CTN at the same reaction condition except usage of different type of catalysts. As shown figure 2.6a, shiny black crystal was obtained after reaction. The morphologies of the both sTP-CTNs was compared by means of scanning electron microscopy (SEM). As shown figure 2.5 and 2.6, original THCN crystal structure maintained after reaction in both case. Unlike the morphologies of Zn-CTN aggregated only on the surface, porous empty space was formed in deep inside of the crystals. (Figure 2.4 d-e and 2.5 c-d) Furthermore, it is revealed in the SEM energy-dispersive X-ray spectrum (EDXS) that 5.09 wt.% of zinc chloride remained in Zn-CNTs even after going through the same work-up procedure with the CTN-0. (Figure 2.6e and Table 2.2)

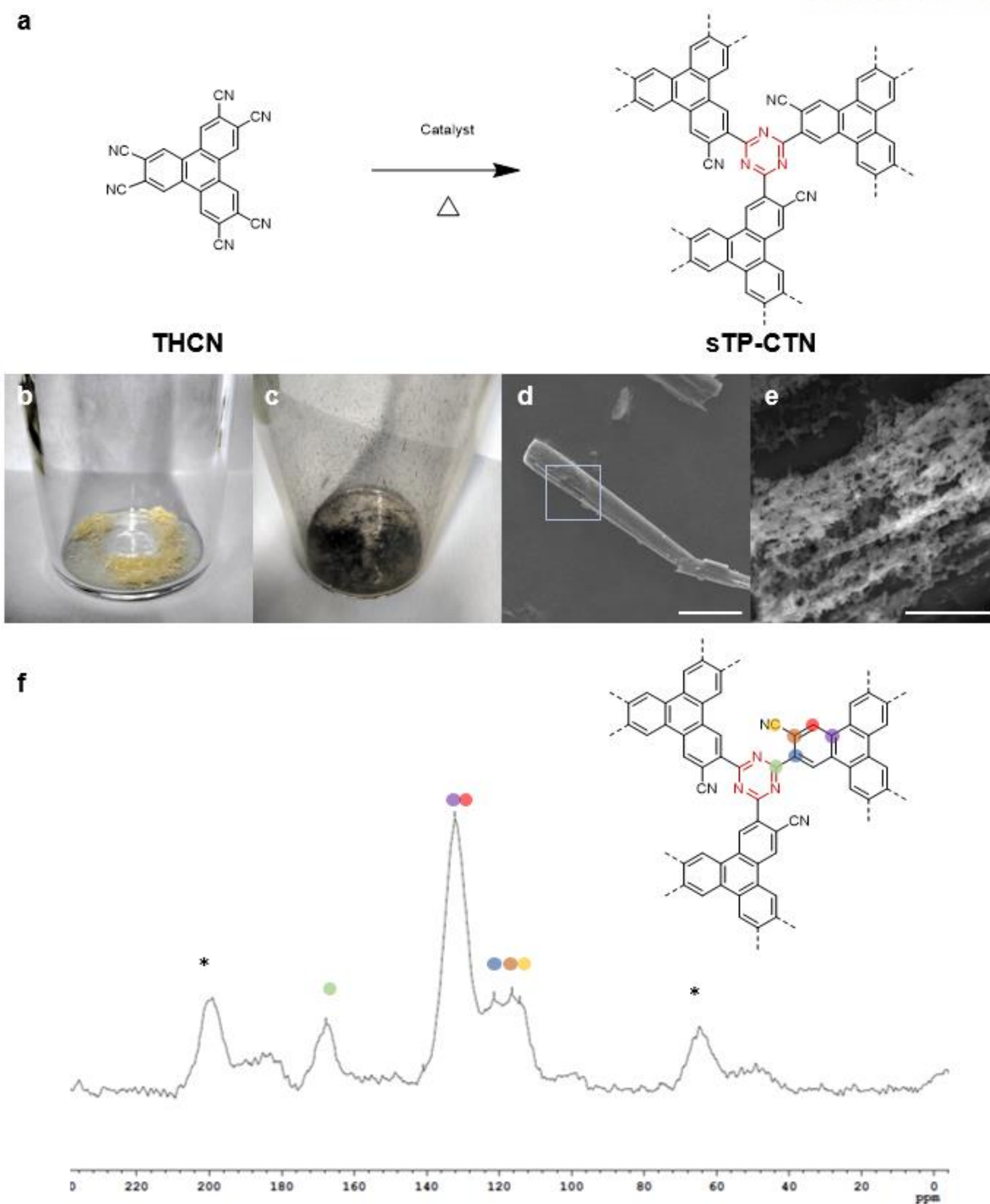


**Figure 2.4.** Synthesis of triphenylene-based conjugated triazine network polymer via solid-state polymerization of THCN (sTP-CTN). (a) Schematic representation of sTP-CTN formation in the presence of hydrochloric acid gas. Digital photographs of (b) THCN crystals and (c) after synthesis of CTN-0 at 450 °C. SEM image of (d-e) CTN-0 at different scale. (Scale bar: 50  $\mu\text{m}$  and 2  $\mu\text{m}$ .) (f) Solid  $^{13}\text{C}$  NMR spectrum of CTN-0.

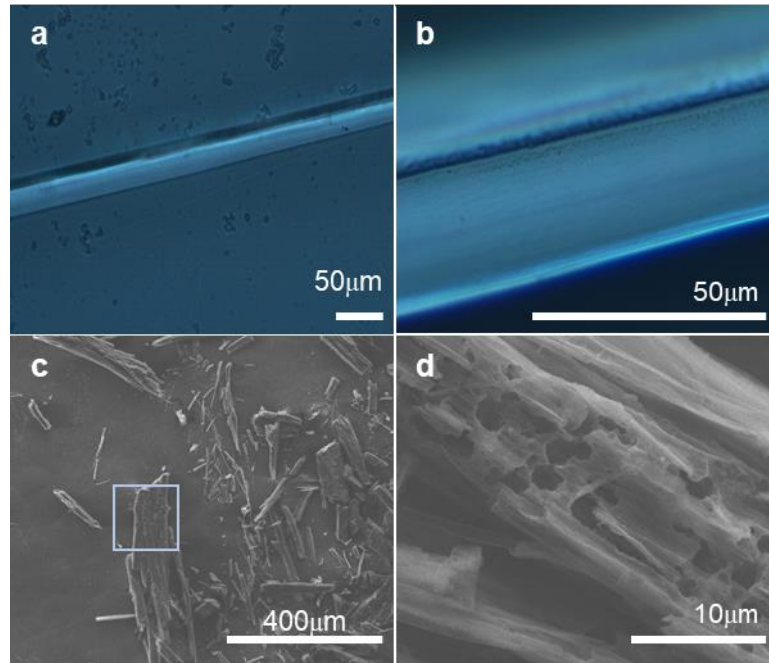


**Figure 2.5.** (a-b) Optical microscopy images of THCN crystals. (c-d) SEM images of CTN-0.

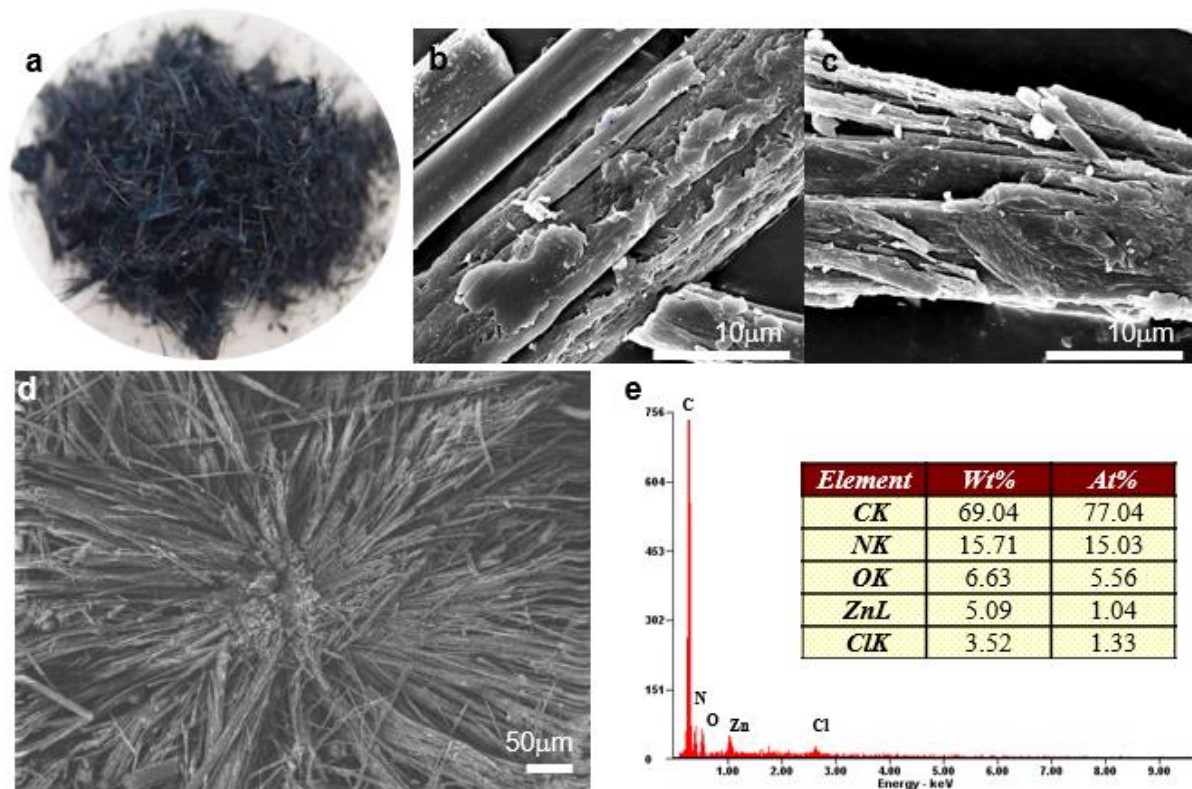


**Figure 2.6.** (a) A digital photograph of Zn-CTN. (b-d) SEM images of Zn-CTN. (e) SEM energy-dispersive X-ray (EDS) spectrum of Zn-CTNs, showing corresponding the contents of element (wt.%).

**Table 2.2.** Elemental compositions of THCN crystals, CTN-0 and Zn-CTN.

	THCN · CH <sub>3</sub> CN		THCN		CTN-0		Zn-CTN	
	Calcd. (wt.%)	EA (wt.%)	Calcd. (wt.%)	EA (wt.%)	Calcd. (wt.%)	EA (wt.%)	Calcd. (wt.%)	XPS (wt.%)
C	76.19	76.34	76.19	76.34	76.19	71.20	76.19	69.04
N	22.21	22.57	22.21	22.57	22.21	16.32	22.21	15.71
O	-	-	-	-	-	10.31	-	6.63
H	1.60	1.50	1.60	1.50	1.60	2.08	1.60	-
Zn	-	-	-	-	-	-	-	5.09
Cl	-	-	-	-	-	-	-	3.52
	100.00	100.41	100.00	100.41	100.0	99.91	100.0	99.99

Fourier-transform infrared spectroscopy (FT-IR) and X-ray photon electron spectroscopy (XPS) were performed to confirm the chemical connectivity and formation of s-triazine. In FT-IR (Figure 2.7a), spectra (Figure 2.7a) were consistent with the expected structure of both CTNs. Unique s-triazine stretching vibration at 1519 and 1380 cm<sup>-1</sup> was observed and the peak at 2236 cm<sup>-1</sup> which was assigned to the C≡N functional group, significantly reduced in CTN-0 and Zn-CTN, indicating that the trimerization of nitrile into s-triazine had occurred in both reaction. The powdered X-ray diffraction (PXRD) patterns showed two broad but intense peaks at the same position in both CTNs, suggesting the existence partially crystalline structures. The peak near 10° indicated by asterisk are assigned rearranged monomer molecules which trapped inside of the triazine networks.

The X-ray photoelectron spectroscopy (XPS) are performed to characterize bonding nature and chemical structure of CTN-0. (Figure 2.8) Three distinct peaks which are corresponding to the presence of C 1s, N 1s and O 1s were observed. The C 1s deconvolution peaks (Figure 2.8b) at 285.0 eV and, 288.3 eV demonstrate that materials possess C-C and C-N carbon bonding and also the peak at 291.1 eV indicated that C=C boning in triphenylene core. Furthermore, high-resolution survey spectra of N 1s showed that three peaks representing pyridinic N (399.3 eV), pyrrolic N (399.6 eV) and quaternary N (401.7 eV)<sup>77-78</sup>. In the O 1s high-resolution XPS survey, C-O, C=O and C-OH peaks were observed which imply that unreacted nitrile functional group hydrolyzed in acidic condition during work-up process. Thermogravimetric analysis (TGA) shows that CTN-0 has almost no weight loss up to 600 °C in nitrogen (N<sub>2</sub>) conditions. Compared to Zn-CTN, TGA thermograms of CTN-0 obtained in air atmosphere showed small weight loss starting around 200 °C and decomposed at approximately 600 °C which has higher thermo-oxidative stability than Zn-CTN.

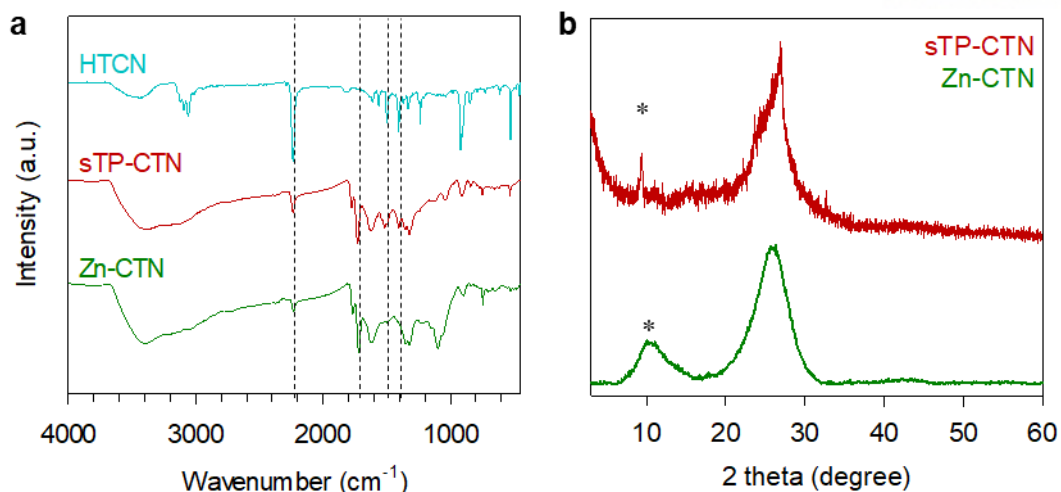


**Figure 2.7.** (a) Fourier transform infrared spectroscopy (FT-IR) spectra of precursor, HTCN and two sTP-CTNs (KBr pellets). The s-triazine of sTP-CTNs vibrated at both 1519 and 1380  $\text{cm}^{-1}$ . (b) X-ray diffraction (XRD) patterns of CTN-0 and Zn-CTN.

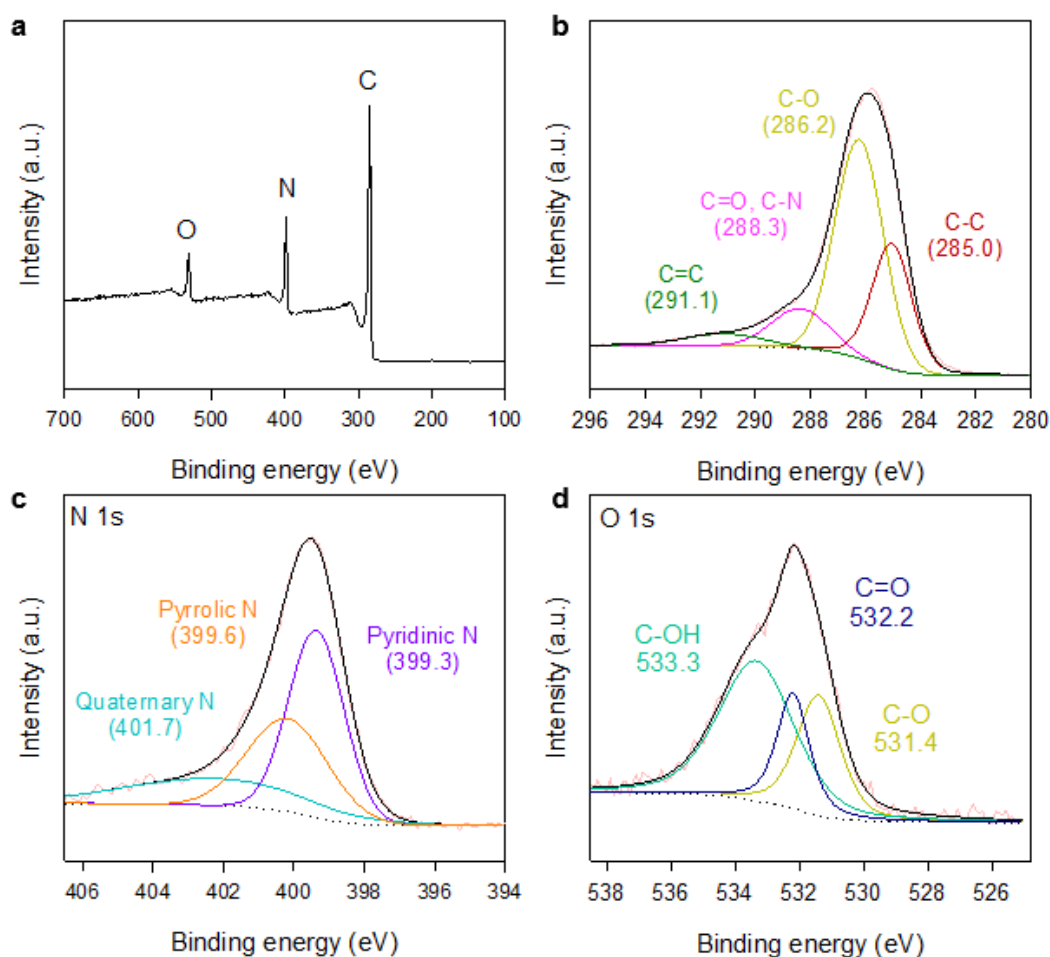


**Figure 2.8.** XPS spectra of CTN-0: (a) Full survey spectra; High-resolution (b) C 1s, (c) N 1s and (d) O 1s spectra.

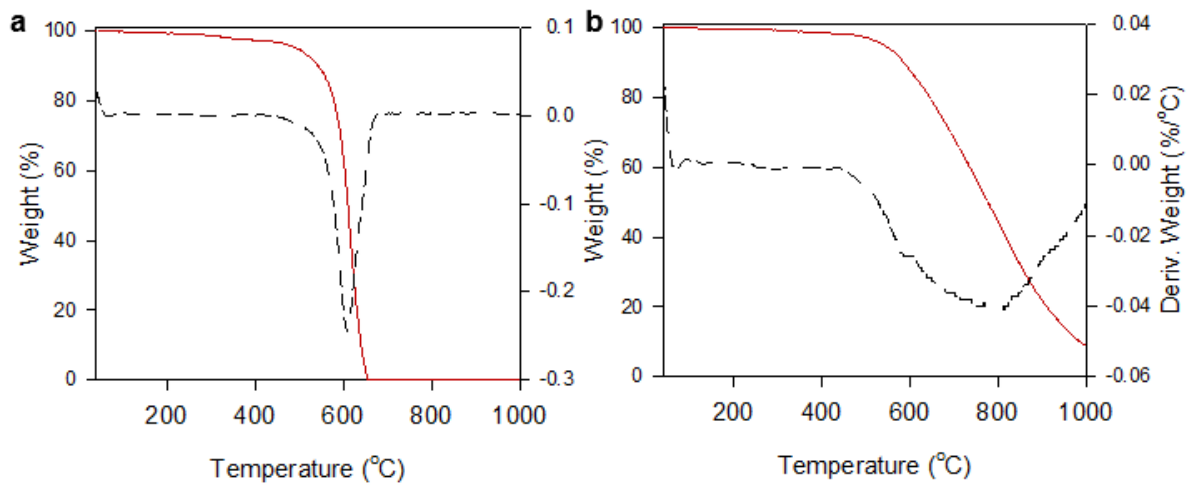


**Figure 2.9** TGA thermograms of CTN-0 crystals with ramping rate of  $10\text{ }^{\circ}\text{C min}^{-1}$ : (a) in air and (b) in nitrogen.

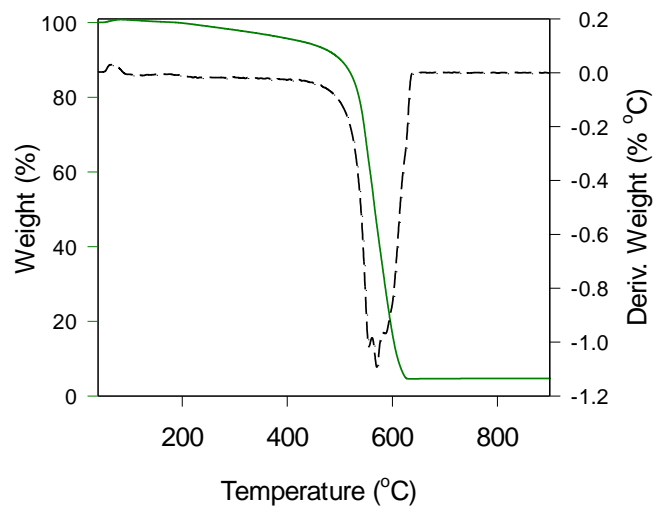


**Figure 2.10.** TGA thermograms of Zn-CTN with ramping rate of  $10\text{ }^{\circ}\text{C min}^{-1}$  in air.



## | Conclusion

In summary, a triphenylene-based conjugated triazine networks (CTN-0) was successfully synthesized by using gaseous hydrogen chloride as a catalyst in solid-state. Newly formed s-triazine in CTN-0 was clearly demonstrated by measuring various analysis and compared with the CTNs synthesized in molten Lewis acid,  $ZnCl_2$ . The CTN-0 prepared in this work provide a new strategy to synthesize triazine-based networks with many advantages over typical methods, for examples, easy work-up process, solvent-free conditions, eco-friendly approach and higher thermo-oxidative stability.

## References

- (1) Roth, W. J.; Nachtigall, P.; Morris, R. E.; Cejka, J. Two-Dimensional Zeolites: Current Status and Perspectives. *Chem. Rev.* **2014**, *114*, 4807-4837.
- (2) Li, J. Y.; Corma, A.; Yu, J. H. Synthesis of new zeolite structures. *Chem. Soc. Rev.* **2015**, *44*, 7112-7127.
- (3) Furukawa, H.; Cordova, K. E.; O'Keeffe, M.; Yaghi, O. M. The Chemistry and Applications of Metal-Organic Frameworks. *Science* **2013**, *341*, 974-985.
- (4) Kitagawa, S.; Kitaura, R.; Noro, S. Functional porous coordination polymers. *Angew. Chem. Int. Ed.* **2004**, *43*, 2334-2375.
- (5) Cote, A. P.; Benin, A. I.; Ockwig, N. W.; O'Keeffe, M.; Matzger, A. J.; Yaghi, O. M. Porous, crystalline, covalent organic frameworks. *Science* **2005**, *310*, 1166-1170.
- (6) Hasell, T.; Cooper, A. I. Porous organic cages: soluble, modular and molecular pores. *Nat. Rev. Mater.* **2016**, *1*.
- (7) Tozawa, T.; Jones, J. T. A.; Swamy, S. I.; Jiang, S.; Adams, D. J.; Shakespeare, S.; Clowes, R.; Bradshaw, D.; Hasell, T.; Chong, S. Y.; Tang, C.; Thompson, S.; Parker, J.; Trewin, A.; Bacsá, J.; Slawin, A. M. Z.; Steiner, A.; Cooper, A. I. Porous organic cages. *Nat. Mater.* **2009**, *8*, 973-978.
- (8) Das, S.; Heasman, P.; Ben, T.; Qiu, S. L. Porous Organic Materials: Strategic Design and Structure-Function Correlation. *Chem. Rev.* **2017**, *117*, 1515-1563.
- (9) Slater, A. G.; Cooper, A. I. Function-led design of new porous materials. *Science* **2015**, *348*, 988-997.
- (10) Mahmood, J.; Lee, E. K.; Jung, M.; Shin, D.; Jeon, I. Y.; Jung, S. M.; Choi, H. J.; Seo, J. M.; Bae, S. Y.; Sohn, S. D.; Park, N.; Oh, J. H.; Shin, H. J.; Baek, J. B. Nitrogenated holey two-dimensional structures. *Nat. Commun.* **2015**, *6*, 6486-6492.
- (11) Mahmood, J.; Lee, E. K.; Jung, M.; Shin, D.; Choi, H. J.; Seo, J. M.; Jung, S. M.; Kim, D.; Li, F.; Lah, M. S.; Park, N.; Shin, H. J.; Oh, J. H.; Baek, J. B. Two-dimensional polyaniline (C3N) from carbonized organic single crystals in solid state. *P. Natl. Acad. Sci. USA* **2016**, *113*, 7414-7419.
- (12) Colson, J. W.; Dichtel, W. R. Rationally synthesized two-dimensional polymers. *Nat Chem* **2013**, *5*, 453-465.
- (13) Zhan, X. J.; Chen, Z.; Zhang, Q. C. Recent progress in two-dimensional COFs for energy-related applications. *J. Mater. Chem. A* **2017**, *5*, 14463-14479.
- (14) Ding, S. Y.; Wang, W. Covalent organic frameworks (COFs): from design to applications. *Chem. Soc. Rev.* **2013**, *42*, 548-568.
- (15) Van Deusen, R. L. Benzimidazo-benzophenanthroline polymers. *J. Polym. Sci. B: Pol. Lett.* **1966**, *4*, 211-214.
- (16) Arnold, F. E. Ladder Polymers Containing Heterocyclic Units of Different Structure. *J. Polym. Sci. Pol. Lett.* **1969**, *7*, 749-753.
- (17) Stille, J. K.; Freeburg, Me Ladder Polyquinoxalines from an Aliphatic Tetraketone. *J. Polym. Sci. Pol. Lett.* **1967**, *5*, 989-992.
- (18) Lee, J.; Kalin, A. J.; Yuan, T. Y.; Al-Hashimi, M.; Fang, L. Fully conjugated ladder polymers. *Chem. Sci.* **2017**, *8*, 2503-2521.
- (19) Scherf, U. Ladder-type materials. *J. Mater. Chem.* **1999**, *9*, 1853-1864.
- (20) Wang, S. H.; Sun, H. D.; Ail, U.; Vagin, M.; Persson, P. O. A.; Andreasen, J. W.; Thiel, W.; Berggren, M.; Crispin, X.; Fazzi, D.; Fabiano, S. Thermoelectric Properties of Solution-Processed n-Doped Ladder-Type Conducting Polymers. *Adv. Mater.* **2016**, *28*, 10764-10771.
- (21) Yohannes, T.; Neugebauer, H.; Luzzati, S.; Catellani, M.; Yi, S.; Jenekhe, S. A.; Sariciftci, N. S. In situ UV-VIS-NIR and Raman spectroelectrochemical studies of the conjugated ladder polymer polybenzimidazobenzophenanthroline (BBL). *Synth. Met.* **2001**, *119*, 319-320.
- (22) Alam, M. M.; Jenekhe, S. A. Efficient solar cells from layered nanostructures of donor and acceptor conjugated polymers. *Chem. Mater.* **2004**, *16*, 4647-4656.
- (23) Borno, P.; Prevot, M. S.; Yu, X. Y.; Guijarro, N.; Sivula, K. Direct Light-Driven Water Oxidation by a Ladder-Type Conjugated Polymer Photoanode. *J. Am. Chem. Soc.* **2015**, *137*, 15338-15341.



(24) Lipomi, D. J.; Chiechi, R. C.; Reus, W. F.; Whitesides, G. M. Laterally Ordered Bulk Heterojunction of Conjugated Polymers: Nanoskiving a Jelly Roll. *Adv. Funct. Mater.* **2008**, *18*, 3469-3477.

(25) Jenekhe, S. A.; Yi, S. J. Highly photoconductive nanocomposites of metallophthalocyanines and conjugated polymers. *Adv. Mater.* **2000**, *12*, 1274-1278.

(26) McAllister, B. T.; Schon, T. B.; DiCarmine, P. M.; Seferos, D. S. A study of fused-ring thieno[3,4-e]pyrazine polymers as n-type materials for organic supercapacitors. *Polym. Chem.* **2017**, *8*, 5194-5202.

(27) Stenger-Smith, J. D.; Lai, W. W.; Irvin, D. J.; Yandek, G. R.; Irvin, J. A. Electroactive polymer-based electrochemical capacitors using poly(benzimidazo-benzophenanthroline) and its pyridine derivative poly(4-aza-benzimidazo-benzophenanthroline) as cathode materials with ionic liquid electrolyte. *J. Power Sources* **2012**, *220*, 236-242.

(28) Mandal, A. K.; Mahmood, J.; Baek, J. B. Two-Dimensional Covalent Organic Frameworks for Optoelectronics and Energy Storage. *Chemnanomat* **2017**, *3*, 373-391.

(29) Chen, L. C.; Zhang, K. C.; Tang, C. Q.; Zheng, Q. D.; Xiao, Y. Controllable and Stepwise Synthesis of Soluble Ladder-Conjugated Bis(Perylene Imide) Fluorenebisimidazole as a Multifunctional Optoelectronic Material. *J. Org. Chem.* **2015**, *80*, 1871-1877.

(30) Babel, A.; Jenekhe, S. A. High electron mobility in ladder polymer field-effect transistors. *J. Am. Chem. Soc.* **2003**, *125*, 13656-13657.

(31) Sun, H.; Vagin, M.; Wang, S.; Crispin, X.; Forchheimer, R.; Berggren, M.; Fabiano, S. Complementary Logic Circuits Based on High-Performance n-Type Organic Electrochemical Transistors. *Adv. Mater.* **2018**, *30*, 1704916.

(32) Zimmerman, C. M.; Koros, W. J. Comparison of gas transport and sorption in the ladder polymer BBL and some semi-ladder polymers. *Polymer* **1999**, *40*, 5655-5664.

(33) Mahmood, J.; Kim, D.; Jeon, I. Y.; Lah, M. S.; Baek, J. B. Scalable Synthesis of Pure and Stable Hexaaminobenzene Trihydrochloride. *Synlett* **2013**, *24*, 246-248.

(34) Jeon, I. Y.; Shin, Y. R.; Sohn, G. J.; Choi, H. J.; Bae, S. Y.; Mahmood, J.; Jung, S. M.; Seo, J. M.; Kim, M. J.; Chang, D. W.; Dai, L. M.; Baek, J. B. Edge-carboxylated graphene nanosheets via ball milling. *P. Natl. Acad. Sci. USA* **2012**, *109*, 5588-5593.

(35) Muckenhuber, H.; Grothe, H. The heterogeneous reaction between soot and NO<sub>2</sub> at elevated temperature. *Carbon* **2006**, *44*, 546-559.

(36) Roberts, J. D.; Caserio, M. C., *Basic Principles of Organic Chemistry: Study Guide*. W. A. Benjamin: 1977.

(37) Figueiredo, J. L.; Pereira, M. F. R.; Freitas, M. M. A.; Orfao, J. J. M. Modification of the surface chemistry of activated carbons. *Carbon* **1999**, *37*, 1379-1389.

(38) Arnold, F. E.; Vanduse. RI Preparation and Properties of High Molecular Weight, Soluble Oxobenz[De]Imidazobenzimidazoisoquinoline Ladder Polymer. *Macromolecules* **1969**, *2*, 497-502.

(39) Roberts, J. D.; Caserio, M. C., *Basic Principles of Organic Chemistry*. California Institute of Technology: 1961.

(40) Scherf, U.; Mullen, K. The synthesis of ladder polymers. *Adv Polym Sci* **1995**, *123*, 1-40.

(41) Arnold, F. E.; Vanduse. RI Unusual Film-Forming Properties of Aromatic Heterocyclic Ladder Polymers. *J. Appl. Polym. Sci.* **1971**, *15*, 2035-2047.

(42) Xie, L. H.; Suh, M. P. High CO<sub>2</sub>-Capture Ability of a Porous Organic Polymer Bifunctionalized with Carboxy and Triazole Groups. *Chem-Eur J* **2013**, *19*, 11590-11597.

(43) Bae, S. Y.; Kim, D.; Shin, D.; Mahmood, J.; Jeon, I. Y.; Jung, S. M.; Shin, S. H.; Kim, S. J.; Park, N.; Lah, M. S.; Baek, J. B. Forming a three-dimensional porous organic network via solid-state explosion of organic single crystals. *Nat. Commun.* **2017**, *8*,

(44) Kato, R.; Nishide, H. Polymers for carrying and storing hydrogen. *Polym. J.* **2018**, *50*, 77-82.

(45) Wang, Q. Y.; Johnson, J. K. Optimization of carbon nanotube arrays for hydrogen adsorption. *J. Phys. Chem. B* **1999**, *103*, 4809-4813.

(46) Jung, S. H.; Kim, H. K.; Yoon, J. W.; Chang, J. S. Low-temperature adsorption of hydrogen on nanoporous aluminophosphates: Effect of pore size. *J. Phys. Chem. B* **2006**, *110*, 9371-9374.

(47) Sumida, K.; Rogow, D. L.; Mason, J. A.; McDonald, T. M.; Bloch, E. D.; Herm, Z. R.; Bae, T. H.; Long, J. R. Carbon Dioxide Capture in Metal-Organic Frameworks. *Chem. Rev.* **2012**, *112*, 724-

781.

(48) Wang, W. J.; Zhouab, M.; Yuan, D. Q. Carbon dioxide capture in amorphous porous organic polymers. *J. Mater. Chem. A* **2017**, *5*, 1334-1347.

(49) Luo, Y. L.; Li, B. Y.; Wang, W.; Wu, K. B.; Tan, B. Hypercrosslinked Aromatic Heterocyclic Microporous Polymers: A New Class of Highly Selective CO<sub>2</sub> Capturing Materials. *Adv. Mater.* **2012**, *24*, 5703-5707.

(50) Fei, H. H.; Bresler, M. R.; Oliver, S. R. J. A New Paradigm for Anion Trapping in High Capacity and Selectivity: Crystal-to-Crystal Transformation of Cationic Materials. *J. Am. Chem. Soc.* **2011**, *133*, 11110-11113.

(51) Kyzas, G. Z.; Fu, J.; Matis, K. A. The Change from Past to Future for Adsorbent Materials in Treatment of Dyeing Wastewaters. *Materials* **2013**, *6*, 5131-5158.

(52) Li, Z. L.; Li, H.; Guan, X. Y.; Tang, J. J.; Yusran, Y. R.; Li, Z.; Xue, M.; Fang, Q. R.; Yan, Y. S.; Valtchev, V.; Qiu, S. L. Three-Dimensional Ionic Covalent Organic Frameworks for Rapid, Reversible, and Selective Ion Exchange. *J. Am. Chem. Soc.* **2017**, *139*, 17771-17774.

(53) Gong, M. Q.; Yu, Q. Y.; Ma, S. Y.; Luo, F.; Wang, R.; Chen, D. Z. Self-Assembly Behavior of Triphenylene-Based Side-Chain Discotic Liquid Crystalline Polymers. *Macromolecules* **2017**, *50*, 5556-5564.

(54) Pal, S. K.; Kumar, S. Novel triphenylene-based ionic discotic liquid crystalline polymers. *Liq. Cryst.* **2008**, *35*, 381-384.

(55) Han, J.; Fan, X.; Zhuang, Z. Z.; Song, W. C.; Chang, Z.; Zhang, Y. H.; Bu, X. H. A triphenylene-based conjugated microporous polymer: construction, gas adsorption, and fluorescence detection properties. *Rsc. Adv.* **2015**, *5*, 15350-15353.

(56) Kuhn, P.; Antonietti, M.; Thomas, A. Porous, covalent triazine-based frameworks prepared by ionothermal synthesis. *Angew. Chem. Int. Ed.* **2008**, *47*, 3450-3453.

(57) Sakaushi, K.; Hosono, E.; Nickerl, G.; Gemming, T.; Zhou, H. S.; Kaskel, S.; Eckert, J. Aromatic porous-honeycomb electrodes for a sodium-organic energy storage device. *Nat. Commun.* **2013**, *4*.

(58) Bohra, H.; Li, P. Z.; Yang, C. J.; Zhao, Y. L.; Wang, M. F. "Greener" and modular synthesis of triazine-based conjugated porous polymers via direct arylation polymerization: structure-function relationship and photocatalytic application. *Polym. Chem.* **2018**, *9*, 1972-1982.

(59) Bojdys, M. J.; Jeromenok, J.; Thomas, A.; Antonietti, M. Rational Extension of the Family of Layered, Covalent, Triazine-Based Frameworks with Regular Porosity. *Adv. Mater.* **2010**, *22*, 2202-2205.

(60) Ren, S. J.; Bojdys, M. J.; Dawson, R.; Laybourn, A.; Khimyak, Y. Z.; Adams, D. J.; Cooper, A. I. Porous, Fluorescent, Covalent Triazine-Based Frameworks Via Room-Temperature and Microwave-Assisted Synthesis. *Adv. Mater.* **2012**, *24*, 2357-2361.

(61) Bavykina, A. V.; Olivos-Suarez, A. I.; Osadchii, D.; Valecha, R.; Franz, R.; Makkee, M.; Kapteijn, F.; Gascon, J. Facile Method for the Preparation of Covalent Triazine Framework coated Monoliths as Catalyst Support: Applications in C1 Catalysis. *Acc. Appl. Mater. Inter.* **2017**, *9*, 26060-26065.

(62) Talapaneni, S. N.; Hwang, T. H.; Je, S. H.; Buyukcakir, O.; Choi, J. W.; Coskun, A. Elemental-Sulfur-Mediated Facile Synthesis of a Covalent Triazine Framework for High-Performance Lithium-Sulfur Batteries. *Angew. Chem. Int. Ed.* **2016**, *55*, 3106-3111.

(63) Soo-Young, Y.; Javeed, M.; Hyuk-Jun, N.; Jeong-Min, S.; Sun-Min, J.; Sun-Hee, S.; Yoon-Kwang, I.; In-Yup, J.; Jong-Beom, B. Direct Synthesis of a Covalent Triazine-Based Framework from Aromatic Amides. *Angew. Chem. Int. Ed.* **2018**, *130*, 1-6.

(64) Hayashi, S.; Togawa, Y.; Ashida, J.; Nishi, K.; Asano, A.; Koizumi, T. Synthesis of pi-conjugated porous polymers via direct arylation of fluoroarenes with three-arm triazine. *Polymer* **2016**, *90*, 187-192.

(65) Breslow, R.; Jaun, B.; Kluttz, R. Q.; Xia, C. Z. Ground-State Pi-Electron Triplet Molecules of Potential Use in the Synthesis of Organic Ferromagnets. *Tetrahedron* **1982**, *38*, 863-867.

(66) R.-A. s. Rapid Auto software, Cat. No. 9220B101, Rigaku Corporation.

(67) G. M. Sheldrick, *Acta Crystallogr. A* **2008**, *64*, 112-122.

(68) Jung, S. M.; Ahn, Y. H. Inflammatory biomarkers in pediatric patients with urinary tract

infection. *Eur. J. Pediatr.* **2016**, *175*, 1736-1736.

(69) Koelsch, C. F.; Whitney, A. G. THE ROSENMUND-von BRAUN NITRILE SYNTHESIS1. *J. Org. Chem.* **1941**, *06*, 795-803.

(70) Julius, v. B.; Gottfried, M. Fluoranthen und seine Derivate. III. Mitteilung. *J. Liebigs Ann. Chem.* **1931**, *488*, 111-126.

(71) W., R. K.; Erich, S. Das am Ringkohlenstoff gebundene Halogen und sein Ersatz durch andere Substituenten. I. Mitteilung: Ersatz des Halogens durch die Carboxylgruppe. *Berichte der deutschen chemischen Gesellschaft (A and B Series)* **1919**, *52*, 1749-1756.

(72) Krempf, H.; Mattmer, R.; Hanack, M. Synthesis of hexacyanotriphenylene and hexacyanotribenzylene. *Synthesis* **2000**, 1705-1708.

(73) Bengelsdorf, I. S. High Pressure-High Temperature Reactions .1. The Trimerization of Aromatic Nitriles. *J. Am. Chem. Soc.* **1958**, *80*, 1442-1444.

(74) Hsu, L. C. Catalytic Trimerization of Aromatic Nitriles for Synthesis of Polyimide Matrix Resins. *Adv. Chem.* **1974**, 145-155.

(75) Zhu, X.; Tian, C. C.; Mahurin, S. M.; Chai, S. H.; Wang, C. M.; Brown, S.; Veith, G. M.; Luo, H. M.; Liu, H. L.; Dai, S. A Superacid-Catalyzed Synthesis of Porous Membranes Based on Triazine Frameworks for CO<sub>2</sub> Separation. *J. Am. Chem. Soc.* **2012**, *134*, 10478-10484.

(76) Grundmann, C.; Kreutzberger, A. Triazines .9. 1,3,5-Triazine and Its Formation from Hydrocyanic Acid. *J. Am. Chem. Soc.* **1954**, *76*, 5646-5650.

(77) Li, Z.; Xu, Z. W.; Wang, H. L.; Ding, J.; Zahiri, B.; Holt, C. M. B.; Tan, X. H.; Mitlin, D. Colossal pseudocapacitance in a high functionality-high surface area carbon anode doubles the energy of an asymmetric supercapacitor. *Energ. Environ. Sci.* **2014**, *7*, 1708-1718.

(78) Hao, L.; Ning, J.; Luo, B.; Wang, B.; Zhang, Y. B.; Tang, Z. H.; Yang, J. H.; Thomas, A.; Zhi, L. J. Structural Evolution of 2D Microporous Covalent Triazine-Based Framework toward the Study of High-Performance Supercapacitors. *J. Am. Chem. Soc.* **2015**, *137*, 219-225.

## Acknowledgement

3년 동안의 대학원 생활을 마치며 주변에 너무나 고마운 분들이 많다는 것을 느꼈습니다. 연구실에서 지낸 여러 날들은 저에게 소중한 경험과 기억이 되었고 학위과정의 시작부터 졸업까지 도움을 주신 많은 분들께 이 자리를 빌어 감사 말씀을 전하고자 합니다.

먼저, 학위 과정 동안 많은 관심과 사랑을 베풀어 주시고 부족한 제가 석사과정을 마칠 수 있도록 많은 조언과 격려로 지도해주신 백종범 교수님께 감사를 드립니다. 든든한 친정이 되어 주시겠다는 응원을 항상 간직하고 언제나 자랑스러운 제자가 되도록 노력하겠습니다. 학사과정을 지도해 주셨던 홍성유 교수님과 졸업발표를 심사해주신 정후영 교수님, 전인엽 교수님께도 감사의 말씀을 올립니다.

3년 동안 그 누구보다도 더 많은 시간을 함께 했던 CDCOF 멤버들과 먼저 졸업하신 선배님과 후배들이 있어 즐겁게 대학원 생활을 할 수 있었습니다. 연구와 개인적인 일에도 조언과 애정을 아끼지 않으셨던 인엽오빠, 후배들을 알뜰 살뜰히 챙겨주는 서윤언니, 내 일처럼 함께 슬퍼해주고 기뻐해 주셨던 선민언니, 처음 입학해 아무것도 모르는 저를 데리고 실험을 가르쳐준 정민언니, 그리고 지금은 졸업하셨지만 언제나 든든한 말언니 현정언니, 감사드려요. I would like to thank Javeed for enthusiastic discussions and advices on my research and career. 대학원 진학을 결심하도록 도와준 동기이자 선배님 석진이, 반전 촌데레 매력의 윤광오빠, 우리의 맥주 요정 수영언니, 뛰어난 말재간의 혁준이와 시크하지만 다정한 성욱이, 샐러드 짝꿍이었던 영현오빠와 랩마스터 종필이, Ishifaq my good friend and earnest coworker, 108동 식구들 부재오빠와 도형오빠. 모두와 함께 연구하고 생활할 수 있어서 따뜻하고 행복한 시간이었습니다.

그리고, 지금의 제가 있을 수 있도록 항상 믿고 응원해주신 부모님과 정신적인 멘토이자 롤모델인 숭, 잘 챙겨주지 못하는 언니를 따라주는 동생 지니. 사랑하는 가족들이 있어 힘든 시기를 잘 넘기고 새롭게 도전할 수 있는 용기를 얻을 수 있었습니다.

멀리 있어 잘 만나지 못하지만, 10여년 동안 내 곁을 지켜 준 배지랑 보배, 대학시절을 더욱더 빛나게 해준 수녀방 친구들 수연이, 한솔이, 주시, 지연언니, 유량이와 혜림이. 밤 산책과 수다를 책임져준 룸메이트 현미. 그 외에도, 학위 과정 동안 많은 도움을 주시고 의지가 되었던 모든 분들에게 깊은 감사를 드립니다. 앞으로도 이 과정에서 배운 것을 잊지 않고 지금까지의 감사에 보답할 수 있는 어엿한 사회인으로 성장하도록 노력하겠습니다.